

JGR Atmospheres

RESEARCH ARTICLE

10.1029/2023JD039337

Key Points:

- Winter sea ice bi-stability is very robust across model parameters, while summer sea ice bi-stability exists in narrower parameter regimes
- Atmospheric feedbacks determine the width of the model sea-ice bi-stability and the CO₂ value at which Arctic sea ice loss occurs
- Longwave feedbacks—a key contributor to the model bi-stability—are driven more by tropospheric temperature than by clouds or moisture

Supporting Information:

Supporting Information may be found in the online version of this article.

Correspondence to:

C. Hankel,
camille_hankel@g.harvard.edu

Citation:

Hankel, C., & Tziperman, E. (2023). Assessing the robustness of Arctic sea ice bi-stability in the presence of atmospheric feedbacks. *Journal of Geophysical Research: Atmospheres*, 128, e2023JD039337. <https://doi.org/10.1029/2023JD039337>

Received 29 MAY 2023
Accepted 18 OCT 2023

© 2023. American Geophysical Union.
All Rights Reserved.

Assessing the Robustness of Arctic Sea Ice Bi-Stability in the Presence of Atmospheric Feedbacks

Camille Hankel¹  and Eli Tziperman^{1,2} 

¹Department of Earth and Planetary Sciences, Harvard University, Cambridge, MA, USA, ²School of Engineering and Applied Sciences, Cambridge, MA, USA

Abstract Arctic sea-ice loss is influenced by multiple positive feedbacks, sparking concerns of accelerated loss in the coming years or even a tipping point, where a sea-ice equilibrium disappears at a given CO₂ value and sea ice rapidly evolves to a new steady state. Such a tipping point would imply a bi-stability of the Arctic climate—where multiple steady-state Arctic climates are possible at the same CO₂ value. Previous works have sought to establish the existence of bi-stability using a range of models, from zero-dimensional sea ice thermodynamic models to fully coupled global climate models, with conflicting results. Here, we present a new model of the Arctic that includes both sea-ice thermodynamics and key atmospheric feedbacks in a simple framework. We exploit the model's simplicity to identify physical mechanisms that control the timing and extent of sea-ice bi-stability, and the abruptness of ice loss. We show that longwave radiation feedbacks can have a strong influence on Arctic surface climate from atmospheric temperature increases alone, even without major contributions from clear-sky moisture or convective clouds suggested previously. While winter sea-ice bi-stability is robust to changes in uncertain model parameters in this study, summer sea ice is more sensitive. Finally, our model indicates that positive feedbacks may modulate the CO₂ threshold of sea-ice loss and the width of bi-stability much more strongly than the abruptness of loss. These results lead to a comprehensive understanding of the conditions that favor Arctic sea-ice bi-stability, particularly the role of atmospheric feedbacks, in both future and past climates.

Plain Language Summary Arctic sea ice is declining rapidly under global warming, threatening high-latitude communities and ecologies. Some mechanisms may cause this sea ice loss to accelerate, leading to concerns about the possibility of a sea ice “tipping point,” in which ice is lost very abruptly and irreversibly at a threshold value of CO₂. Previous works have used a range of tools, from simple sea ice thermodynamic models to state-of-the-art global climate models, to identify whether such a tipping point exists and have found conflicting results. In this work, we present a novel model of the Arctic climate that combines a thermodynamic model of sea ice with atmospheric feedbacks in a simple framework. We run this model across large ranges of climatic conditions to broadly identify the conditions that favor a sea ice tipping point. In addition, we isolate the mechanisms that are key to setting the timing and abruptness of complete sea ice loss, separating the contributions of different atmospheric feedbacks that have previously been unexplored. We find that both summer and winter sea ice tipping points are possible and that the responsible atmospheric mechanisms are different than those that have been suggested previously.

1. Introduction

Arctic sea ice is already observed to be rapidly declining (Comiso & Parkinson, 2004; Nghiem et al., 2007; Notz & Stroeve, 2016; Stroeve & Notz, 2018; Stroeve et al., 2008), sparking concerns over the possibility of a “tipping point” in sea ice loss in the future as anthropogenic warming continues. Such a tipping point—defined as an abrupt fall in total sea ice at some threshold value of CO₂—could be caused by a transition from a CO₂ range that supports multiple steady-state values of sea ice to one that supports only one steady-state. This transition (mathematically referred to as a “bifurcation,” see Ghil & Childress, 1987; Strogatz, 1994) would also imply irreversibility of sea ice loss, meaning that CO₂ concentrations would have to decrease below the value at which sea ice collapsed to recover the sea ice cover. This scenario has severe policy implications, and as such, a large body of literature has emerged seeking to establish whether bi-stability in Arctic sea ice (multiple steady-states for the same CO₂ forcing) exists.

Previous studies have used a variety of different modeling tools to answer the question of Arctic bi-stability and have found different, often conflicting results. Simple thermodynamic models of sea ice that include the ice-albedo feedback and ice-thickness growth feedback but exclude dynamic atmospheric feedbacks and processes find no or limited bi-stability in summer sea ice (i.e., no bifurcation/tipping point when transitioning from perennial to seasonal sea ice cover), but do find a small CO₂ range of bi-stability in winter sea ice (i.e., a tipping point in the transition from seasonal ice cover to ice-free conditions, Abbot et al., 2011; Eisenman, 2007, 2012; Eisenman & Wettlaufer, 2009; Notz, 2009). When such a sea ice model is coupled to an energy balance atmospheric model with a resolved latitudinal dimension, meridional heat diffusion destroys the sea-ice bi-stability (Wagner & Eisenman, 2015). On the other hand, in an atmospheric column model that includes sea ice and realistic atmospheric feedbacks, the winter sea-ice bifurcation re-emerges and is associated with bi-stability between a convecting and non-convecting atmospheric state (Abbot & Tziperman, 2008). In fully coupled global climate models (GCMs) the picture becomes even less clear. In GCMs run under the RCP8.5 Scenario in CMIP5, three of the seven models that lose their winter sea ice by the end of the simulations show an abrupt loss of winter sea ice (Hankel & Tziperman, 2021; Hezel et al., 2014) that is characteristic of, but not exclusively explained by, a bifurcation and the associated sea ice bi-stability. Holland et al. (2006) identified possible abrupt jumps in summer sea ice, but Holland et al. (2008) concluded this was likely not related to a tipping point. On the other hand, Ferreira et al. (2011) found bi-stability between ice-free and perennially ice-covered conditions in an intermediate complexity GCM. Moreover, other studies that have directly tried to test for bi-stability in GCMs by running hysteresis experiments (Armour et al., 2011; Li et al., 2013; Ridley et al., 2012) have been unable to conclusively identify or rule out the existence of sea ice bi-stability because it is computationally infeasible to simulate the sea ice steady-state at many different CO₂ values in such models.

Additionally, there has been some debate over what sets the abruptness of Arctic sea ice loss, particularly with respect to the loss of winter (seasonal) sea ice. While a bifurcation in the sea ice steady state necessarily implies an extremely abrupt loss of ice, it is not the only plausible cause of abruptness (Lenton, 2012). Some studies (e.g., Bathiany et al., 2016) suggest the freezing point of seawater creates a natural threshold that is sufficient for abrupt sea ice loss, while others (Hankel & Tziperman, 2021) show that local positive feedback mechanisms set the range of abruptness in sea ice loss across GCMs. It is thus unclear what the relative importance of different mechanisms is in contributing to abrupt sea ice loss, leading to uncertainty in understanding the physical and mathematical mechanisms behind climate model predictions of future ice loss.

Given that the previous literature on Arctic bi-stability has used many different models with different components, parameter choices, and assumptions, it is hard to pinpoint what physical mechanisms and modeling choices favor/destroy Arctic bi-stability and thus hard to reconcile the range of results. We, therefore, identify a need to study Arctic climate bi-stability under many different conditions within *the same model* to build a more general and robust understanding of what controls Arctic bi-stability and the abruptness of Arctic sea ice loss. This will not only allow us to re-interpret some of this past work in a clear, unified framework but will also provide a comprehensive assessment of the key local mechanisms that influence Arctic climate transitions and their relative importance.

The motivation for this study is twofold. First, a mechanistic understanding of the factors controlling the abruptness of sea ice loss with future anthropogenic warming will help us better interpret the large intermodel spread of sea ice predictions made by GCMs. Second, a general understanding of the climatic conditions that influence Arctic bi-stability will shed light on past climates. In particular, the climate during the warm period of the Eocene was very different from today, including potentially different ocean stratification and heat transport, and different natural aerosols, which could influence cloud feedbacks. All of these factors could alter the nature of Arctic bi-stability. Given that the Eocene had a warm initial condition (in the sense that it was cooling down from a much hotter Cretaceous), investigating how these factors influence Arctic bi-stability may aid the understanding of the relationship between climate, sea ice, and CO₂ during this period. We do not explore the effect of possible time-dependent CO₂ fluctuations during the period, as might have occurred during the Paleocene-Eocene thermal maximum, for example.

To achieve these goals, we use a novel model of sea ice—the first box model to include both sea ice and explicit atmospheric radiation feedbacks in a simple framework—which allows us to explore the modeling choices, boundary conditions, and physical mechanisms that cause the Arctic to exhibit bi-stability for a given CO₂ concentration. The model consists of a simple sea ice thermodynamic model (similar to that of Eisenman (2007)

and Eisenman and Wettlaufer (2009)) coupled to a two-layer atmosphere that has parameterizations of convection, longwave radiative cloud and clear-sky effects, and air-sea heat exchanges. This is a key addition compared to energy balance models that typically include an atmosphere assumed to be in radiative equilibrium with the surface, and in which the parameterized longwave feedback parameter is prescribed. Thus, our model contains representations of most of the key atmospheric feedbacks that have been proposed to influence sea ice loss and retains the computational efficiency and interpretability afforded by a box model. Importantly, it also allows us to directly manipulate atmospheric processes (through mechanism denial experiments, and modifying parameterizations) in ways that are not feasible in a GCM or even in an atmospheric column model.

We first use this model to exhaustively sweep broad ranges of parameters that are not well-constrained in past and future warm climates and which have not been explored together in previous studies (including CO₂, cloud emissivity, ocean mixed-layer depth, meridional ocean heat transport). Next, we perform mechanism denial experiments (e.g., suppressing the surface albedo feedback (SAF), turning off different aspects of the longwave feedbacks) to reveal what mechanisms modulate the abruptness and CO₂ threshold for sea ice loss in the present-day climate.

We find that in every scenario, the SAF seems to be necessary for any bi-stability; the convective cloud feedback and clear-sky longwave feedbacks cannot introduce bi-stability on their own. However, we find that a subset of our model parameters, while unable to produce bi-stability without the SAF, can significantly widen or shift the range of CO₂ values for which there is bi-stability. In particular, we find that longwave feedbacks significantly shift the CO₂ value at which sea ice is lost and do so mostly through changes in tropospheric temperature, rather than through convective clouds or water vapor feedbacks as has been suggested previously (Abbot & Tziperman, 2008; Abbot et al., 2009). This suggests that developing an understanding of these parameters and mechanisms in a future climate is crucial for predicting abrupt transitions in Arctic sea ice cover.

In mechanism denial experiments, we find that sea ice loss can still be somewhat abrupt even when no bi-stability and bifurcation occur. Generally, we see that local positive feedback mechanisms have a much greater influence on the CO₂ threshold of sea ice loss than on the abruptness of such loss. This means evaluating the strength of these feedbacks in the present-day climate is key for predicting the CO₂ threshold at which the Arctic is ice-free: a prediction that still exhibits significant intermodel spread in GCMs.

2. Methods

In this section, we describe the ice-ocean-atmosphere model we use. There are eight prognostic variables in the system: ocean mixed layer temperature (T_o), sea ice volume (V), sea ice fraction (f_{SI}), sea ice surface temperature (T_{SI}), atmospheric boundary layer temperature (T_b), atmospheric boundary layer moisture (q_b), tropospheric temperature (T_a), and tropospheric moisture (q_a). The model represents one grid box in the Arctic with an area of 1 km by 1 km, though our results do not depend on the chosen grid box size.

2.1. Oceanic and Atmospheric Temperature Equations

The rate of change of the temperature of the tropospheric layer, T_a , is a function of (from left to right in Equation 1): longwave upwelling from the surface, latent heat from water vapor condensing into precipitation, radiative cooling of the layer, convective heat flux from the boundary layer, heat transport from the midlatitudes, and large-scale subsidence,

$$\frac{dT_a}{dt} = \frac{g}{\Delta p_{ATM} c_p^{air}} [\epsilon(1 - f_{SI})\sigma T_o^4 + \epsilon f_{SI}\sigma T_{SI}^4 + \rho_{water} L_e P_a - 2\epsilon\sigma T_a^4] + \frac{\Delta p_{BL}}{\Delta p_{ATM}} F_{c,a} + \frac{T_{mid,a} - T_a}{\tau_a} + S. \quad (1)$$

Here, S is a prescribed temperature tendency due to subsidence, $T_{mid,a}$ is the tropospheric temperature of the midlatitudes, $F_{c,a}$ is a convective heat flux, P_a is the rate of precipitation from the atmospheric layer in meters per second, and ϵ is the emissivity of the atmosphere, given in Equation (4). We neglect shortwave absorption by the atmosphere for simplicity and because we expect its effect on the feedback processes studied here to be negligible. In particular, (Hankel & Tziperman, 2021) found that shortwave absorption by the atmosphere can act

as a negative feedback on the surface Arctic climate due to enhanced SW absorption by water vapor in a warmer climate, but this feedback was very small compared to negative feedbacks from surface turbulent heat fluxes and longwave feedbacks. All other physical and modeling parameters in the above equation and their default values can be found in Tables S1–S4 of the Supporting Information S1. Precipitation occurs when the tropospheric relative humidity passes a fixed threshold, and is defined in Section 2.2. $F_{c,a}$, the convective heat flux into the atmospheric layer, is nonzero only when a raised boundary layer parcel is buoyant compared to the tropospheric layer. The convective heat flux is given by,

$$F_{c,a} = \begin{cases} (T_p - T_a)/\tau_c & T_p > T_a, \\ 0 & \text{otherwise,} \end{cases} \quad (2)$$

where T_p is the temperature of a boundary layer parcel after being lifted to the tropospheric level, and τ_c is a convective mixing timescale. This parcel temperature is obtained by solving the following the moist static energy conservation equation,

$$\begin{aligned} M S E_b &= c_p T_b + g z_b + L_e q_b \\ &= c_p T_p + g z_a + L_e \min(q_b, q_s(T_p)) \\ &= M S E_p, \end{aligned}$$

where all a subscripts correspond to the atmospheric (troposphere) layer and all b subscripts correspond to the atmospheric boundary layer. The timescale τ_c depends on the efficiency of convection and is given by,

$$\tau_c = \left[\frac{\Delta T}{T_p - T_a} \right] \tau_M, \quad (3)$$

where ΔT is a reference temperature difference between the parcel and the atmosphere, set to 10 K, and τ_M is a reference convective mixing timescale, set to 3 hr (see Table S2 in Supporting Information S1).

The emissivity of the atmosphere, ϵ , is a function of CO_2 , water vapor concentration, and longwave forcing due to convective clouds, given by,

$$\epsilon = \epsilon_0 + 0.041 \times \log_2(\text{CO}_2/280 \text{ ppm}) + 0.072 \times \max(0, \log_2(q_a/q_0)) + \Delta\epsilon_{cl}, \quad (4)$$

where $\Delta\epsilon_{cl}$, the change in emissivity due to clouds, is defined below in Section 2.4 (Tziperman, 2022).

The rate of change of the temperature of the surface atmospheric boundary layer (T_b) is a function of sensible heat fluxes from the surface, latent heating from condensing precipitation, a convective heat flux, heat flux from the midlatitudes, and the same prescribed subsidence heating from Equation 1,

$$\begin{aligned} \frac{dT_b}{dt} &= \frac{g}{\Delta\rho_{BL}c_p^{air}} [(1 - f_{SI})(T_o - T_b)C + f_{SI}(T_{ice} - T_b)C + \rho_{water}L_e P_b] \\ &\quad - F_{c,b} + \frac{T_{mid,BL} - T_b}{\tau_a} + S \end{aligned} \quad (5)$$

Precipitation (P_b) is defined below in Section 2.2. The convective heat flux ($F_{c,b}$, a heat flux out of the boundary layer when convection is active) is given by,

$$F_{c,b} = \begin{cases} (T_b - \theta_a)/\tau_c & T_p > T_a, \\ 0 & \text{otherwise,} \end{cases} \quad (6)$$

where θ_a is the potential temperature of the atmospheric parcel brought to the level of the boundary layer. The constant C is a surface drag coefficient used for calculating the surface sensible heat flux. We set it to $C = \rho_{air}\nu_H c_p^{air} C_w$ where ν_H is the surface wind speed, and C_w is a transfer coefficient between the ocean surface and the atmosphere (see Table S2 in Supporting Information S1 and Sayag et al., 2004), following the ocean-atmosphere heat parameterization in the Community Atmosphere Model version 5 (the Community Earth

System Model guide; Neale et al., 2010). Because the atmospheric boundary layer is relatively thin (it represents the lower 200 hPa) and tightly coupled to the surface temperature, we ignore longwave transmission in this layer, as it would likely absorb and re-emit radiation from the surface at nearly the same temperature and provide no greenhouse effect.

The rate of change of the ocean mixed layer temperature (T_o) is affected by shortwave radiation directly absorbed by the open ocean, longwave cooling, evaporation at the surface, sensible heat exchange with the atmospheric boundary layer, LW downwelling radiation from the atmosphere, heat exchange with the bottom of the sea ice including the effects of melting and freezing, and heat transport from the warmer mid-latitudes,

$$\frac{dT_o}{dt} = \frac{1}{D} \frac{1}{\rho_o c_p^{water}} (1 - f_{SI}) [SW(y)(1 - \alpha_{atm})(1 - \alpha_o) - \sigma T_o^4 - C_w v_H L_e \rho_{air} \{q_s(T_o) - q_b\} - (T_o - T_b)C + \epsilon \sigma T_a^4] + F_{IO} + \frac{T_{mid,o} - T_o}{\tau_o}. \quad (7)$$

Here D is the ocean mixed layer depth, α_{atm} is the atmospheric albedo, α_o is the ocean albedo, and $T_{mid,o}$ is the temperature of the midlatitude ocean. The shortwave forcing (SW) is an approximation of the seasonal cycle of insolation that depends on latitude (y) according to Hartmann (2015). F_{IO} is the heat exchange between the ocean and sea ice (if present) given by,

$$F_{IO} = \begin{cases} -(T_o - T_f)/\tau_f & T_o < T_f, \\ -f_{SI} \times (T_o - T_f)/\tau_f & \text{otherwise.} \end{cases} \quad (8)$$

The above conditional means that if the ocean temperature is below freezing it will warm back to freezing as sea ice forms, and if it is above freezing it will be cooled by the ice above it in proportion to how much ice is present.

The saturation specific humidity ($q_s(T)$), used to determine surface evaporation in Equation 7 above and in the moisture equations later, is given by the Clausius Clapeyron relation (Emanuel, 1994),

$$q_s(T) = 2(.622e_s/p_o)e^{-L_e/(R_v T)}. \quad (9)$$

2.2. Moisture Equations

The rate of change of the specific humidity of the tropospheric layer, q_a , is determined by a moisture flux due to convection, precipitation that removes moisture, and a moisture flux from the mid-latitudes,

$$\frac{dq_a}{dt} = \frac{\Delta p_{BL}}{\Delta p_{ATM}} Q_{c,a} - \frac{g}{\Delta p_{ATM}} P_a \rho_{water} + \frac{q_{mid,a} - q_a}{\tau_a}. \quad (10)$$

The midlatitude moisture flux above is a function of the midlatitude temperature while assuming a fixed relative humidity of the midlatitudes and is given by $q_{mid,a} = RH_{atm} \times q_s(T_{mid,a})$. The precipitation rate is given by,

$$P_a = \begin{cases} \frac{1}{\tau_p} \frac{\Delta p_{ATM}}{g \rho_{water}} [q_a - R q_s(T_a)] & q_a > R q_s(T_a), \\ 0 & \text{otherwise.} \end{cases} \quad (11)$$

Here, R is the relative humidity threshold that triggers precipitation, and $Q_{c,a}$, the convective moisture flux, is defined similarly to the convective heat flux as follows,

$$Q_{c,a} = \begin{cases} (q_p - q_a)/\tau_c & T_p > T_a \\ 0 & \text{otherwise,} \end{cases} \quad (12)$$

where $q_p = \min(q_b, q_s(T_p))$ is the specific humidity of the convecting parcel coming from the boundary layer, which may or may not be saturated.

The rate of change of the specific humidity of the boundary layer is determined by evaporation and precipitation close to the surface, convective moisture transport upward, and moisture transport from the mid-latitudes,

$$\frac{dq_b}{dt} = \frac{g}{\Delta p_{BL}} [C_w \nu_H \rho_{air} \{q_s(T_o) - q_b\} (1 - f_{SI}) - P_b \rho_{water}] - Q_{c,b} + \frac{q_{mid,BL} - q_b}{\tau_a}, \quad (13)$$

where $q_{mid,BL}$ is defined similarly to $q_{mid,a}$ above, and P_b is the precipitation rate in the boundary layer, similarly defined as the rate in the atmosphere as,

$$P_b = \begin{cases} \frac{1}{\tau_p} \frac{\Delta p_{BL}}{g \rho_{water}} [q_b - Rq_s(T_b)] & q_b > Rq_s(T_b), \\ 0 & \text{otherwise.} \end{cases} \quad (14)$$

The convective moisture flux out of the boundary layer is not necessarily equal to the flux into the tropospheric layer due to condensation, and is defined similarly to that in the tropospheric layer as,

$$Q_{c,b} = \begin{cases} (q_b - q_a)/\tau_c & T_p > T_a, \\ 0 & \text{otherwise.} \end{cases} \quad (15)$$

2.3. Sea Ice Equations

There are three prognostic sea ice variables: total volume (V), ice area fraction (f_{SI}), and the temperature of the surface of the sea ice (T_{SI}). If T_{SI} is above freezing and the total net surface flux (described below) into the ice is positive, then the ice can both melt at the surface and at the ice-ocean interface. Otherwise, ice only grows/melts according to the energy balance at the bottom of the ice. These two cases are treated separately in the equations provided below. The net sea ice surface flux (positive downward) is,

$$F_{sfc} = SW(y)(1 - \alpha_{atm})(1 - \alpha_{ice}) + \sigma \epsilon T_a^4 - \sigma T^4 + (T_b - T_{SI})C, \quad (16)$$

where the terms represent solar radiation absorbed by the ice, longwave downwelling radiation from the atmosphere, longwave cooling by the ice, and sensible heat exchange with the atmospheric boundary layer, respectively. Thus if $T_{SI} \geq 0$ and $F_{sfc} > 0$, the ice volume and temperature evolve according to,

$$\frac{dV}{dt} = \left(c_p^{water} \rho_{water} D \Delta x \Delta y F_{IO} - A_{ice} (SW(y)(1 - \alpha_{atm})(1 - \alpha_{mp}) + \sigma \epsilon T_a^4 - \sigma T^4 + (T_b - T_{SI})C) \right) \frac{1}{L_f \rho_{ice}}, \quad (17)$$

$$\frac{dT_{SI}}{dt} = 0, \quad (18)$$

where A_{ice} is the ice area calculated as the ice fraction times the size of the horizontal model domain, and all other constants are given in Table S4 of the Supporting Information S1. In Equations 17 and 18, all surface heating goes into melting ice while the ice surface temperature stays at the melting point. The first term of Equation 17 is the ice-ocean heat exchange at the bottom of the ice defined in Section 2.1, and the rest of the terms are as in Equation 16 for F_{sfc} except the surface albedo of the ice is modified to a melt pond albedo value (α_{mp}).

In the other case, when the surface melting condition is not met, ice volume changes are dictated only by the heat budget at the bottom of the ice, determined as a balance between ice-ocean heat exchanges and vertical heat conduction through the ice, and the ice surface temperature evolves due to heat conduction through the ice and surface heat fluxes.

$$\frac{dV}{dt} = \left(c_p^{water} \rho_{water} D \Delta x \Delta y F_{IO} - A_{ice} \frac{c_p^{ice} \rho_{ice} \kappa (T_{SI} - T_f)}{H_{ice}} \right) \frac{1}{L_f \rho_{ice}}, \quad (19)$$

$$\frac{dT_{SI}}{dt} = \left(\frac{-c_p^{ice} \rho_{ice} \kappa (T_{SI} - T_f)}{H_{ice}} + F_{sfc} \right) \frac{1}{h_{sfc} c_p^{ice} \rho_{ice}}, \quad (20)$$

where H_{ice} is the ice thickness (volume divided by area), and $h_{sfc} = 10$ cm is the depth of ice near the surface whose temperature responds to surface fluxes according to Equation 20. Finally, ice fraction evolves according to Eisenman (2007), with all new ice growth being given a characteristic small thickness (H_{min}) that contributes to entirely to lateral ice growth. Ice volume loss contributes to ice area loss through a different proportionality constant that approximately reproduces the observed thickness distribution (Hibler, 1979). The equations are,

$$\frac{df_{SI}}{dt} = \begin{cases} \frac{dV}{dt} \frac{1}{H_{min} \Delta x \Delta y} & \text{if } \frac{dV}{dt} > 0, \\ \frac{f_{SI}}{2V} \frac{dV}{dt} & \text{otherwise.} \end{cases} \quad (21)$$

If dV/dt is positive and f_{SI} has already reached its maximum value of 1, then df_{SI}/dt is set to zero, and the volume growth leads to a thickening of the ice only.

2.4. Clouds

Low clouds are not parameterized directly, and thus we cannot study the influence of shortwave cloud feedbacks on Arctic bi-stability. Low clouds have been proposed as a possible negative feedback on Arctic climate, whereby summer sea ice loss could fuel enhanced low cloud cover in the summer, which would reduce total insolation reaching the surface and reduce further sea ice loss directly and by through damping the strength of the SAF (Kay et al., 2016). However, many studies have found this proposed summertime negative shortwave cloud feedback to be nonexistent or relatively small both in GCMs (Kay et al., 2012; Morrison et al., 2019) and in observations (Kay & Gettelman, 2009; Kay et al., 2016). We still explore the effect that low clouds might have on the model results by modifying the atmospheric SW albedo, denoted as α_{atm} (see Table S2 in Supporting Information S1).

The effect of high convective clouds on LW emissivity is set to be a function of the convective moisture flux ($Q_{c,b}$) and is calculated as,

$$\Delta \epsilon_{cld} = \Delta \epsilon_0 \max \left(1, \frac{Q_{c,b}}{\Delta Q} \right), \quad (22)$$

where $\Delta \epsilon_0$ and ΔQ are parameters representing the maximum LW effect of clouds and the typical convective moisture flux scale, set to $\Delta \epsilon_0 = 0.2$ and $\Delta Q = 0.0002/\tau_c$ g/kg.

Finally, in addition to affecting the emissivity of the atmosphere, CO_2 also affects the modeled climate through an increase to all midlatitude temperatures (ocean mixed layer, atmospheric boundary layer, and tropospheric layer) by a prescribed amount per each doubling of CO_2 (see Table S2 in Supporting Information S1). The model is implemented in Python 3.7; details of the numerical integrations to a seasonal steady-state climate can be found in Supporting Information S1.

2.5. Experimental Design

In the following subsections, we outline the different types of experiments we run using our coupled model.

2.5.1. 1D Parameter Sweeps

In order to provide a preliminary assessment of the model's sensitivity to different parameters, we perform "1D" parameter sweeps by running the model with many values of one parameter while keeping all other parameters at their default value. Every parameter combination is run in six different conditions: with CO_2 values of 280, 460, and 560 ppm, and with a cold (ice-covered) and warm (ice-free) initial condition to test for the existence of bi-stability. In every case, we run the model until a steady state is reached as described in Supporting Information S1, and use the final year of the integrations to analyze the seasonal cycles of all state variables and diagnostic quantities in the Results.

2.5.2. 2D Parameter Sweeps

From the results of all 1D parameter sweeps (see Tables S2–S4 in Supporting Information S1), we identify a much smaller subset of parameters to which the model steady-state is significantly sensitive. We then run “2D” parameter sweeps, varying the given parameter and CO₂ concentration together. We record the steady-state seasonal cycle of all the simulations, categorizing each into one of three possible steady-states: perennial ice coverage (ice fraction never drops to zero throughout the year), seasonal ice coverage (ice fraction is zero at some point during the year and nonzero at another point), and perennially ice-free (ice fraction is zero year-round).

2.5.3. Mechanism Denial Experiments

We perform several mechanism denial experiments to assess the contribution of different processes to the abruptness of Arctic sea ice loss. First, we conduct a variety of experiments that assess the contribution of longwave feedback processes. We turn off the clear-sky water-vapor feedback, by removing the term from the emissivity equation that depends on the atmospheric specific humidity. Separately, we turn off the convective cloud feedback by setting $\Delta\epsilon_{\text{cld}} = 0$: in other words, eliminating the effect that convection has on the atmospheric emissivity. We also turn off convection entirely, by setting the convective heat and moisture fluxes between the tropospheric and surface boundary layer to zero even if a raised boundary layer parcel is buoyant. In each of the above experiments, however, some longwave feedbacks are still possible through processes that warm the tropospheric layer which in turn increases the longwave downwelling radiation at the surface, even if atmospheric emissivity were fixed. Thus we also perform an experiment that suppresses longwave temperature feedbacks, where atmospheric emissivity has all its components (CO₂, cloud emissivity, and water vapor), but the atmospheric temperature used to calculate longwave downwelling radiation that reaches the surface is fixed to its daily seasonal climatology calculated at 280 ppm of CO₂. We then also suppress all LW feedbacks together by suppressing the temperature feedback as just described and removing the water vapor and cloud contributions from atmospheric emissivity. In this experiment, longwave downwelling radiation received by the surface only changes due to changes in CO₂ concentration. Finally, we suppress the SAF by setting all surface albedo values (ice, melt pond, and ocean) to the same value of 0.6; this value is chosen so that the preindustrial climate still has a reasonable steady-state seasonal cycle of sea ice.

2.6. Model Validation

In order to assess our model's ability to represent a realistic Arctic climate, we compare our model variables at pre-industrial (“PI”) and twice pre-industrial (“2xPI”) CO₂ levels to a state of the GCM from the Coupled Model Intercomparison Project Version 6. We pick one of the GCMs, CanESM5, that most closely matches the seasonal cycle of total Arctic sea ice area observed during the satellite era (Keen et al., 2021). In using such a GCM for our model validation, we can compare our model to a realistic Arctic climate while also being able to make our comparison at different CO₂ levels (PI and 2xPI) which would not be possible using an observational data set. Further details on how the seasonal cycle of CanESM5 data is calculated can be found in Supporting Information S1.

In Figure S1 in Supporting Information S1 we compare the eight state variables of our simple model run with 280 ppm of CO₂ to those of the GCM in a pre-industrial control climate. The seasonal cycle of ice fraction in our model matches closely that of the GCM; this is because we tuned the simple model to match this variable. The seasonal cycle of effective ice thickness and ice surface temperature both qualitatively track those of the GCM. The ocean temperature appears to have a very qualitatively different seasonal cycle than that of the GCM, however, we note that these differences are only on the order of 0.1 K and represent small fluctuations around the freezing temperature. The atmospheric boundary layer and tropospheric layers' temperatures have similar magnitudes of the seasonal cycle to those of the GCM, and are off in absolute value by at most ~5 K. The specific humidity of both layers is also realistic, in particular capturing the more muted seasonal cycle of humidity in the upper atmosphere found in the GCM.

As seen in Figure S2 of the Supporting Information S1, at the 2xPI climate the toy model produces reasonable seasonal cycles of all variables that match those of the GCM. One difference is that the GCM simulates a smoother and more symmetric seasonal cycle of ice fraction than our simple model; this is likely in part because the GCM seasonal cycle represents an average over many grid points (as described in Supporting Information S1), while the simple model contains only one grid box in which sea ice fraction tends to grow and melt

very abruptly during the seasonal cycle. This difference propagates into other variables including tropospheric and boundary layer temperature, boundary layer specific humidity, and ice surface temperature, all of which show realistic magnitudes but more seasonally asymmetric behavior than the GCM as they depend heavily on the presence/absence of ice. In particular, the boundary layer moisture in our model shows sharp changes not found in the GCM that are due to the sudden onset of convection that moves moisture from the boundary layer to the troposphere. The qualitative seasonal cycle of ocean temperature of the simple model matches the GCM well but is biased cold by 1–3 K. CanESM5 did not report ice thickness in the abrupt CO₂ doubling experiment.

While our primary goal is to study local feedback mechanisms in the Arctic, we also evaluate our model's ability to represent remote processes. In twentieth-century observations, poleward transport of dry static energy is on the order of 2PW at 60 N, which comes out to 60 W/m² of heating in the Arctic (Yang et al., 2015). In the PI configuration, our model has about 55 W/m² of heating due to poleward sensible heat fluxes in both atmospheric layers combined. At a 2xPI climate, the poleward sensible heat flux may decline by about 0.1 PW or 3 W/m² (Yoshimori et al., 2017); in our model, it declines by closer to 12 W/m² due to the high level of Arctic amplification in our model.

Historical poleward latent heat fluxes are on the order of 0.5 PW, or 15 W/m² (Yang et al., 2015). Our model under-represents this transport slightly, at 10 W/m² in the PI configuration. Furthermore, while GCMs tend to predict a modest increase in poleward latent heat fluxes of around 6 W/m² (e.g., Yoshimori et al., 2017), our model predicts almost no change in poleward latent heat flux. This is because the default configuration of the model does not lead to preferential moistening of the midlatitudes since moisture in the Arctic box is coupled tightly to surface conditions and increases significantly when sea ice is lost. While the total changes in poleward energy transport into the Arctic under global warming are thought to be or near-zero or negative (e.g., Hwang et al., 2011; Kay et al., 2012; Skific & Francis, 2013, and ours are modestly negative), our model does not capture the important compensation between decreases in dry static energy transport and latent heat transport (Graversen & Burtu, 2016; Graversen & Langen, 2019; Yoshimori et al., 2014). While the direct heating by these two terms through atmospheric heat convergence in the Arctic may approximately cancel out (see Figure 4a of Hahn et al., 2021), the increase in moisture transport leads to additional surface warming indirectly through enhanced cloud feedbacks and the greenhouse effect of water vapor (Graversen & Langen, 2019). Thus, one caveat of this study is that our model's default configuration cannot represent the potential influence of remote energy fluxes on local (particularly cloud and water vapor) feedbacks. Later, we discuss how this may affect our results.

3. Results

In the following sections, we analyze model runs configured with standard parameter values (Section 3.1), the robustness of bi-stability to large changes in modeling parameters (Section 3.2), and the relative importance of different mechanisms in setting the abruptness of sea ice loss (Section 3.3). Throughout the text, we refer to “winter” sea ice as the ice conditions around the time of the annual ice maximum, which can in fact occur as late in the year as April or May, and “summer” sea ice as the conditions around the time of the annual ice minimum, which tends to occur around September.

3.1. Bi-Stability of Sea Ice in the Standard Parameter Regime

We first run the model with default parameter values (see Tables S2–S4 in Supporting Information S1) with a pre-industrial CO₂ concentration (280 ppm). Figure 1 shows the seasonal cycle of all eight prognostic variables of the model for the cold initial condition. At this CO₂ level, there is no bi-stability (there is only one steady-state), so the warm initial condition leads to an identical seasonal cycle to that shown. The previous section on the validation of our model against a realistic GCM indicates that all eight state variables take on realistic values for the Arctic. The tropospheric, boundary layer, and ice surface temperatures (panel c) all exhibit strong seasonal cycles, while the ocean mixed layer temperature stays close to freezing year-round as it is mostly ice-covered. The atmospheric boundary layer moisture increases rapidly when the ice fraction drops below 1 in the summertime due to increased evaporation from the ocean, and the tropospheric layer shows a similar, but more muted response (panel d).

In Figures 2a–2d and 2e–2h we see the model variables again, but for simulations with 530 ppm of CO₂ and cold and warm initial conditions, respectively. We chose to show the results at 530 ppm because it is a canonical

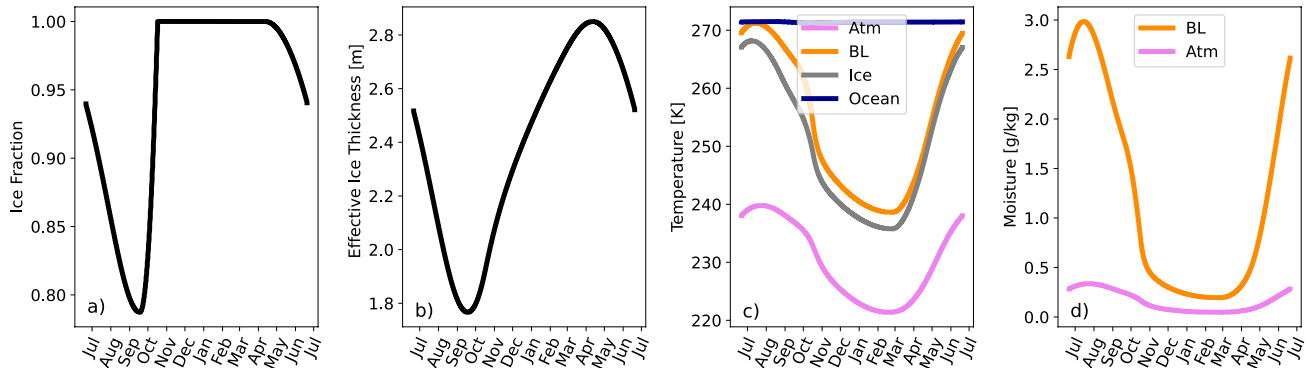


Figure 1. Steady-state seasonal cycle of all eight prognostic variables for a standard (default parameters) pre-industrial run (280 ppm) with a cold initial condition. The abbreviation “Atm” refers to the tropospheric layer of the atmosphere, and “BL” refers to the atmospheric boundary layer. The same simulation run with a warm initial condition leads to the same climate at this CO₂ value.

example of bi-stability that occurs for our default model configuration; the two rows of Figure 2 show very different climates. In the first row, we see that the cold initial condition leads to an Arctic that is ice-free in the summer but still reaches an ice fraction of 1 in the winter. In the simulation that starts with a warm, ice-free initial condition (Figure 2 bottom row), on the other hand, the climate is ice-free year-round, never developing ice due to physical mechanisms that operate differently in the two ICs, as we will discuss shortly. By 655 ppm (not shown), both initial conditions lead to perennially ice-free, identical climates, indicating the limited range of Arctic bi-stability, the robustness of which will be discussed in the next section.

The main features of the bi-stability at 530 ppm are summarized in Figure 3 by showing the different contributions to the surface heat budget. In the analysis below, we consider how six different fluxes—shortwave

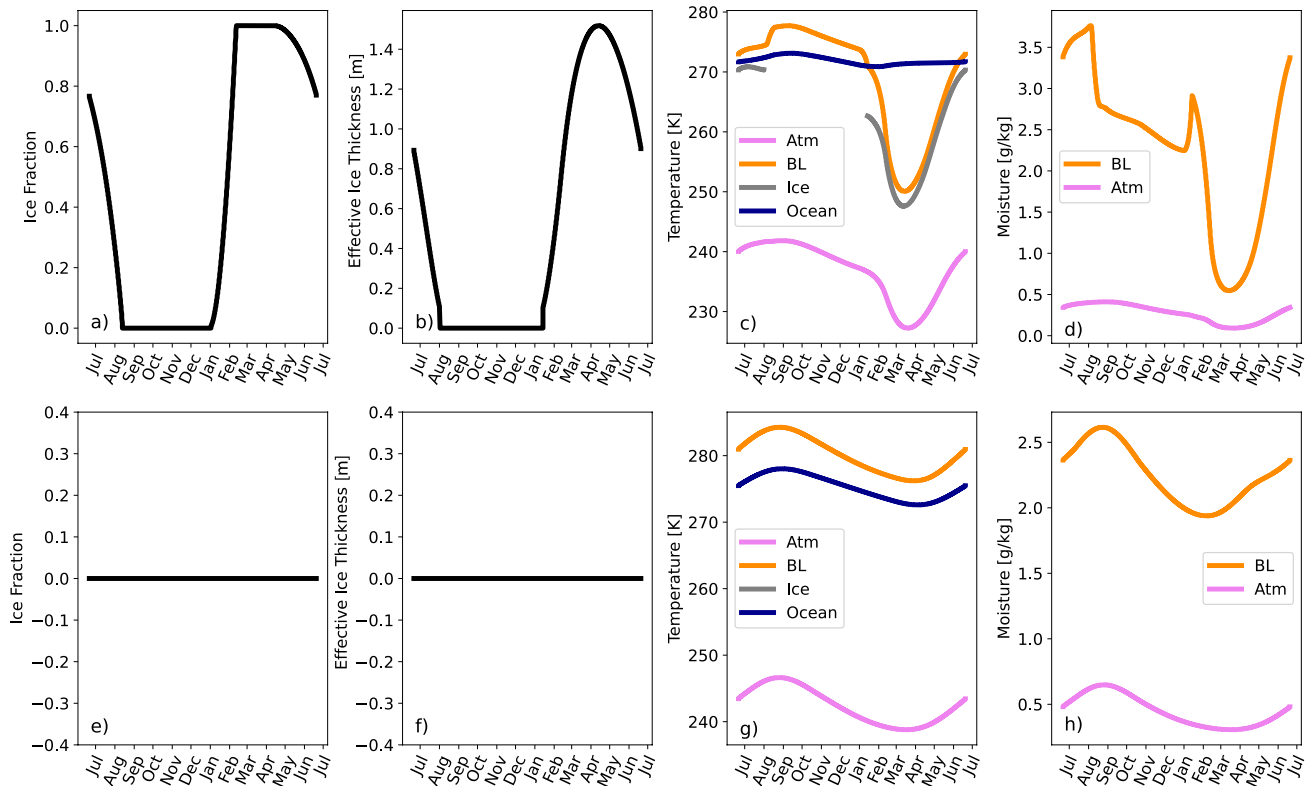


Figure 2. Steady-state seasonal cycle of all eight prognostic variables for an intermediate-warming run (530 ppm). The top row (a–d) shows the steady state of a run initialized with a cold initial condition, and the bottom row (e–h) shows the steady state of a run with a warm initial condition. Because the two rows exhibit different climates, there is bi-stability for the default parameters at this CO₂ concentration.

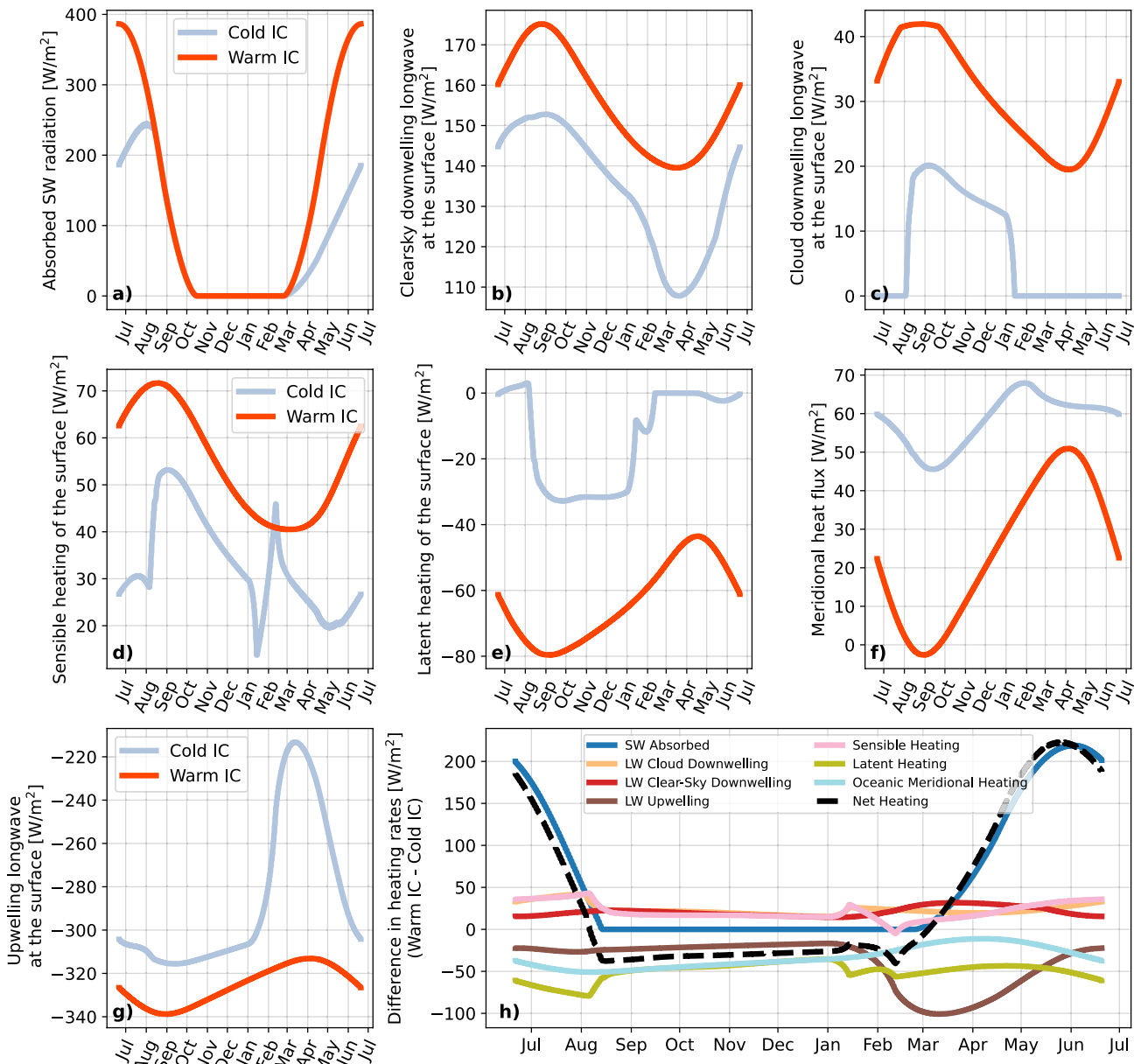


Figure 3. Comparison of all heat fluxes affecting the surface (ice-covered and open ocean areas combined) during the 530 ppm CO_2 runs with cold and warm initial conditions. Positive values indicate heating of the surface and negative values indicate cooling. In panel (h), the differences in heating rates between the warm and cold initial conditions for all the fluxes are plotted together.

radiation, clear-sky and cloud downward longwave radiation, sensible heating, latent cooling, and oceanic meridional heating—contribute to differences between the steady state surface temperatures obtained from the two initial conditions (bi-stability), and the seventh term, longwave upwelling, to represent the surface temperature's response to these six fluxes. Thus, while all seven fluxes must integrate to zero over one seasonal cycle in the steady state, treating the longwave upwelling as a response to, rather than a component of, the surface heat budget allows us to gain insight into the causes of Arctic bi-stability.

Figure 3a shows the shortwave radiation absorbed by the surface, which is the surface heat flux with the largest magnitude. We see that in the warm initial condition simulation (dark orange line), the surface receives substantially more shortwave radiation in the summertime than the cold initial condition (blue line) due to the SAF. Importantly, however, this feedback has its peak contribution to differences in surface heating between the two initial conditions from the months of April to August, when the high latitudes receive sunlight. On the other

hand, the bi-stability in Arctic sea ice at this CO_2 occurs from January to August, potentially suggesting that other processes are needed to explain the sea ice bi-stability during the months that receive no sunlight.

In Figures 3b and 3c, we see the clear-sky and cloud components of longwave downwelling radiation at the surface. While the difference between the warm and cold initial condition longwave heating does not reach the same maximum magnitude as the difference in shortwave heating, it is importantly nonzero during the winter months, with clear-sky longwave radiation contributing about a 30 W/m^2 difference in heating from March to May, and cloud longwave radiation contributing about 20 W/m^2 from January to July. Thus the total longwave heating can contribute around 50 W/m^2 of additional heating in the winter months of the warm initial condition compared to the cold initial condition steady-state, helping to maintain the winter sea-ice bi-stability.

The other surface heat fluxes besides the longwave and shortwave fluxes also contribute to the bi-stable seasonal cycle. In Figure 3d, we see that sensible heating of the surface (which is proportional to the difference between surface temperature and the boundary layer potential temperature) is $10\text{--}30 \text{ W/m}^2$ larger in the warm initial condition run. In panel (e), we see that latent cooling of the surface acts to reduce the surface temperature difference between the two steady-states because the warm initial condition experiences more cooling due to evaporation over the open ocean (Boeke & Taylor, 2018; Hankel & Tziperman, 2021). In panel (f) we see that the ocean meridional heat flux for the two initial conditions, which is represented as a slow relaxation of the Arctic Ocean temperature to a single prescribed midlatitude ocean temperature, acts to push the solution to the two initial conditions toward the same steady state (as it heats the cold IC more than the warm IC). The sign of this feedback matches that found in studies using more complex models (Bitz et al., 2005; Ferreira et al., 2011; Wagner & Eisenman, 2015), although their corresponding mechanisms are different because they resolve a meridional structure of the ocean heat transport. In Figure 3g, we see that the steady state of the warm initial condition run has a larger magnitude of upwelling longwave radiation due to the negative Planck feedback.

Finally, Figure 3h summarizes the relative importance of the six heating terms discussed above by comparing the difference between the two initial conditions for all of them on the same plot. The shortwave radiation is by far the largest magnitude difference term in the summer, while the clear-sky and cloud longwave radiation are the largest difference during most of the sea-ice growth months from January to April. Latent heat fluxes are the largest year-round process warming the cold initial condition much more than the warm initial condition, especially during the winter ice-growth months. However, the meridional ocean heat flux contributes a similar magnitude to suppressing differences in the two initial conditions during the summer and autumn. The black line in Figure 3h shows the sum of all the heating term differences (excluding the Planck feedback's LW upwelling term). This mirrors the findings of previous studies (Boeke & Taylor, 2018; Hahn et al., 2021; Hankel & Tziperman, 2021) that have explained winter Arctic surface warming in GCMs through similar ocean heat storage mechanisms, again demonstrating our model's ability to represent realistic Arctic climate dynamics. While these previous studies showed that this inter-seasonal heat storage mechanism contributed to inter-model differences (in GCMs) in Arctic warming and abrupt sea ice loss, perhaps hinting at a connection to climate bi-stability and tipping points, here we are able to show that it explicitly contributes to year-round climate bi-stability of the Arctic.

To summarize, for this parameter combination (default model parameters and 530 ppm of CO_2), summer sea ice bi-stability does not occur, while winter sea ice bi-stability does because, taken all together, mechanisms that enhance differences between the two initial conditions (causing them to reach different steady states) are stronger in the winter than in summer. The key feedbacks driving the difference between summer and winter sea ice behavior are the shortwave and longwave radiative feedbacks. While one might assume that the shortwave ice-albedo feedback may affect summer sea ice bi-stability more than winter, the peak of insolation is approximately equally offset from the months of ice loss for the two seasons (September and March) making this mechanism effective in both the summer and winter seasons, and possibly even stronger in winter due to seasonal ocean heat storage. Longwave feedbacks, which we later find to be key for maintaining bi-stability across a wide range of CO_2 , contribute to differences between the two initial conditions more strongly in the wintertime than in the summer (Figures 3b and 3c). Together, these feedbacks favor winter bi-stability more than summer bi-stability of sea ice.

3.2. Sea-Ice Winter and Summer Bi-Stability in Broad Parameter Regimes

In this section, we examine the robustness of Arctic climate bi-stability to specific model parameter values. Doing so allows us to: (a) understand the fundamental mechanisms controlling Arctic bi-stability, and (b) gain insight

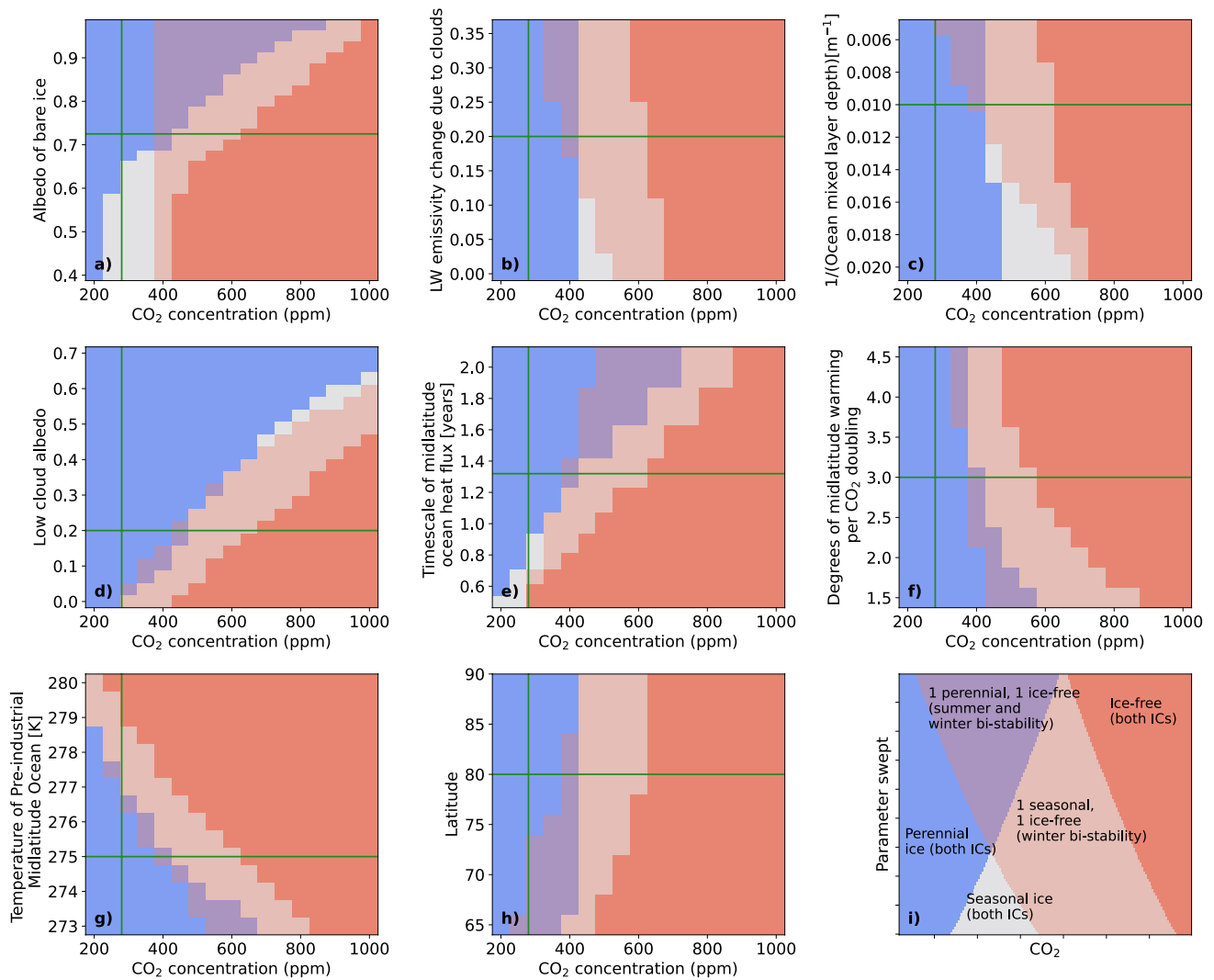


Figure 4. Bifurcation diagram showing parameter regimes that have perennial ice coverage in blue, seasonal ice coverage in white, perennial open ocean in red, and bi-stable states as mixes of two colors. For example, the light pink color indicates a bi-stability where the cold initial condition leads to seasonal ice coverage and the warm initial condition leads to ice-free conditions. The green line indicates the default value of the model parameter. The bottom right panel (i) is a schematic demonstrating the meaning of each contour color.

into how Arctic climate transitions could be different in past/future climates. To do this, we run 2D parameter sweeps (see Section 2) where we vary a given model parameter together with CO₂ and run the model for every parameter combination starting with a cold initial condition and a warm initial condition. The results are shown in Figure 4: blue indicates a steady-state climate with year-round ice coverage, white indicates seasonal ice coverage (ice-free in summer), and red indicates perennial ice-free conditions. Mixes of the colors indicate bi-stability between the two steady states of the seasonal cycle (obtained from the above two initial conditions). Specifically, the bi-stability of winter sea ice described in Figure 2 where the cold initial condition develops seasonal (winter) ice coverage and the warm initial condition develops year-round ice-free conditions, is seen here as the mixed red/white (pink) color. Bi-stability between perennial ice coverage and perennial ice-free conditions (i.e., bi-stability of both summer and winter sea ice simultaneously) is shown in the mixed blue/red (purple) color. The meanings of all colors are indicated in the schematic panel (i) of Figure 4. The magnitudes of the winter and summer sea ice bi-stabilities (meaning the absolute difference in ice fraction between the cold and warm initial conditions) can be found in Figures S3 and S4 in Supporting Information S1 respectively.

Starting in Figure 4a, we show the dependence of ice bi-stability on the bare ice albedo—a key parameter in setting the strength of the ice-albedo feedback. At lower bare ice albedos (0.4–0.575), a small range of CO₂ values

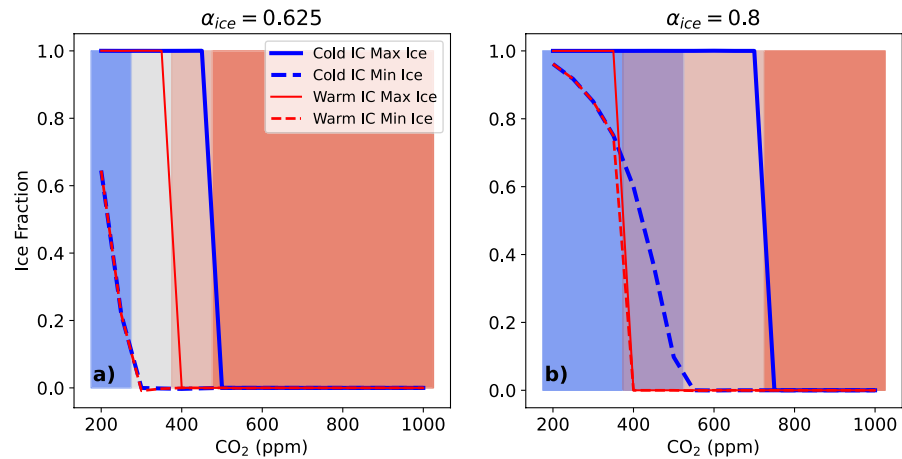


Figure 5. Example of the changing sea ice regimes when bare ice albedo (α_{ice}) increases. The solid lines indicate the maximum (winter) sea ice fraction during the year, and dashed lines indicate the minimum (summer) sea ice. In panel (a), there is only bi-stability of winter sea ice: red and blue lines (indicating the two initial conditions) lie directly on top of each other for the minimum ice value (dashed) but trace a hysteresis loop for the maximum winter ice value (solid). In panel (b), summer sea-ice bi-stability emerges: a hysteresis loop of the dashed line (summer sea ice) lies within the hysteresis loop of the solid line (winter sea ice). Shaded backgrounds indicate the color that each state appears as in Figure 4.

leads to winter bi-stability (white/red mixed color); the warm initial condition never develops sea ice, while the cold initial condition has seasonal (winter) ice. The CO_2 width of this bi-stability increases as the bare ice albedo increases (i.e., the pink color widens as we move up in the plot). This can be explained by two factors. First, the CO_2 threshold at which ice develops in the warm initial condition is completely insensitive to the value of bare ice albedo, as seen by the vertical line at 400 ppm dividing the red-tinted regions on the right side of panel (a) from other regimes. This is because when starting from a warm, ice-free initial condition, the ice-albedo parameter doesn't play a role in the model equations until after an initial amount of ice has developed. Second, for the cold initial condition, the increase in bare ice albedo means that winter ice can be maintained for higher and higher CO_2 values. At ice albedos of 0.7 and above (including our default value indicated by the horizontal green line), a region of bi-stability between perennial ice coverage and perennial ice-free conditions occurs (mixed blue/red color). This indicates bi-stability for both summer and winter ice and implies a hysteresis in CO_2 for both seasons (explained further below). This bi-stability can be explained similarly to the bi-stability of winter sea ice alone: again, the CO_2 threshold for ice development in the warm initial condition still remains unchanged, even at very high ice albedo values, while the increase in ice albedo means the cold initial condition can now support ice year-round (rather than just in winter) at higher CO_2 values.

This summer sea ice bi-stability (that occurs simultaneously with winter sea-ice bi-stability) has been identified in previous studies (Eisenman, 2012; Eisenman & Wettlaufer, 2009) using idealized sea ice models without atmospheric feedbacks. Our default parameter combination leads to a much narrower CO_2 range supporting summer sea-ice bi-stability than those studies, suggesting that the inclusion of additional atmospheric feedbacks may not favor summer bi-stability. While the ice-albedo values that lead to summer sea-ice bi-stability are on the higher end of the realistic range, we will see in the following sections that modestly modifying several other parameters from our default configuration can also produce this bi-stability over larger CO_2 ranges, suggesting that it could occur in the real world under the right conditions.

To illustrate these different regimes more clearly and to show the resulting hysteresis loops in cases of bi-stability, we show maximum and minimum yearly ice values versus CO_2 for both initial conditions and for two example ice albedo values in Figure 5. In Figure 5a, a low value of ice albedo leads to winter sea ice bi-stability, which can be seen as the hysteresis loop traced by the solid lines for over a small range of CO_2 values, while the summer sea ice still shows the same equilibrium value for both initial conditions. On the other hand, at a high ice albedo value (Figure 5b) the additional bi-stability of summer sea ice leads to a narrow summer hysteresis loop (indicated by the loop traced by the dashed lines) which sits entirely within the winter hysteresis loop. The insensitivity of the CO_2 threshold for warm initial condition ice formation to the bare ice albedo choice can be seen as the jump of the solid red line from 1 to 0 occurring in both plots at 400 ppm of CO_2 .

Next, in Figure 4b, we show the effect of varying the LW emissivity enhancement due to convective clouds ($\Delta\epsilon_0$, see Equation 22 in Section 2). Increasing this LW convective cloud emissivity makes the overall climate warmer since it increases LW heating at the surface when convection is active; we see this in the shift of the bi-stable and ice-free regimes to lower values of CO_2 as we move upward through the contour plot. We first note that winter sea-ice bi-stability (pink and purple colors) occurs for the entire range of convective cloud emissivities, indicating that it is a very robust feature of our model. Summer sea ice bi-stability also occurs (concurrently with winter sea-ice bi-stability) for high enough values of $\Delta\epsilon_0$ (0.175 and above), indicated by the purple color. Bi-stabilities in both seasons occur because the transition from perennial to seasonal ice coverage in the cold initial condition is relatively insensitive to $\Delta\epsilon_0$, since convection largely does not occur until after sea ice starts to disappear. On the other hand, for the warm, ice-free initial condition, convection occurs year-round over open ocean, and thus increasing $\Delta\epsilon_0$ warms the surface and shifts the ice-free and seasonal ice regimes to lower CO_2 values for that initial condition.

We now consider how the width of winter sea-ice bi-stability (i.e., the CO_2 range over which the purple and pink colors extend) changes as a function of convective cloud emissivity. This width increases as $\Delta\epsilon_0$ increases, but only slightly. The rather modest dependence of winter bi-stability width on $\Delta\epsilon_0$ makes sense because the positive convective cloud feedback increases warming in the warm initial condition more than in the cold initial condition (due to convection over the ice-free ocean), but as we saw in Figure 3, other factors such as the clear-sky longwave feedback were equally important in explaining bi-stability. Given that the emissivity of convective clouds in the Arctic is very uncertain even in coupled GCMs, the relative insensitivity of the winter bi-stability to $\Delta\epsilon_0$ supports the robustness of winter sea-ice bi-stability. On the other hand, the existence of summer sea-ice bi-stability is highly sensitive to this uncertain parameter, making its existence in the real climate similarly uncertain.

In Figure 4c we show the sea-ice bi-stability as a function of the ocean mixed layer depth, which is plotted as a reciprocal to reflect the quantity that is relevant to the model equations (parameter D in Equation 7). Increasing ocean mixed layer depth makes the overall climate warmer, and increases the width of both summer and winter bi-stability slightly by warming the warm initial condition more than the cold initial condition. The reason for the increase in bi-stability width can be understood as follows: the main process that prevents the warm initial condition from reaching a seasonally ice-covered steady-state is the difficulty in developing winter ice for the first time. Once such sea ice develops, the ice-albedo feedback kicks off and establishes a steady seasonal cycle with consistent winter ice after a few years. Because the warm initial condition is initialized with no sea ice, the low-albedo open ocean absorbs heat all summer long, and must subsequently release enough heat the following winter to reach the freezing temperature and develop sea ice. An increase in ocean mixed layer depth means that the ocean can store more heat in the summer, and subsequently may not be able to release the excess heat in winter to reach the freezing temperature. Crucially, the cold initial condition starts off ice-covered, reflecting more of the late spring/early summer insolation due to a higher surface albedo. Thus while the cold initial condition also sees an increase in summer ocean heat storage with increased mixed layer depth, it is of a smaller magnitude than the increase for the warm initial condition due to the SW radiation being reflected by the sea ice. The differing cold and warm initial condition sensitivities to ocean mixed layer depth explain why the sea ice bi-stability width is sensitive to this key parameter, which is practically unconstrained for past climates.

Figure 4d shows the sea ice steady-states as the atmospheric albedo, which crudely represents the presence of low clouds in the summertime (see Section 2, Equations 7 and 17). Here, we see that increasing low cloud albedo makes the climate colder, as expected, but barely affects the width of sea-ice bi-stability. This is somewhat surprising given that increasing atmospheric albedo should lower the magnitude of the ice-albedo feedback, which is one of the main causes of the sea-ice bi-stability. The insensitivity of the bi-stability width to atmospheric albedo can be explained by two competing effects of an increase in this parameter. First, because the surface albedo of the warm initial condition is low while the surface albedo of the cold initial condition is high, an increase in atmospheric albedo should cool the warm initial condition more than the cold initial condition. However, the cooling of the cold initial condition leads to a small increase in the ice area, which in turn makes the surface albedo even higher, leading to additional cooling of the cold initial condition. These effects approximately offset each other, making the cold and warm ICs similarly sensitive to atmospheric albedo, and thus the width of sea-ice bi-stability relatively insensitive to atmospheric albedo.

In Figure 4e, we find that the width of sea-ice bi-stability is highly sensitive to the restoring timescale used in our simplified mid-latitude ocean heat flux representation. The bi-stability width decreases and eventually

disappears for shorter timescales due to the damping implied by our simple formulation. These findings may indicate that a decrease in ocean heat transport due to the projected weakening of the Atlantic Meridional Overturning Circulation under global warming could influence sea-ice bi-stability. Previous work also found that heat transport by the ocean can act as a negative feedback (Tziperman et al., 1994), and prevent bi-stability (Wagner & Eisenman, 2015). On the other hand, Ferreira et al. (2011) found in a GCM that the meridional structure of ocean heat transport could play a role in supporting bi-stability rather than destroying it.

In Figure 4f, we see that changing the degrees of mid-latitude warming per CO₂ doubling (which represents the mid-latitude climate sensitivity) does not qualitatively alter the sea ice stability regimes. (We note that the apparent disappearance of summer bi-stability around 3.25° per doubling is likely just an artifact of the coarse resolution in CO₂.) Rather, increasing the climate sensitivity merely warms the model more quickly and condenses the bi-stability regimes (both summer and winter) to a smaller range of CO₂. This is to be expected because the model mostly experiences warming due to CO₂ increases through the climate sensitivity of the mid-latitudes rather than directly through increases to the emissivity of the local atmosphere (as in, changing CO₂ without changing midlatitude temperatures would not warm the model very much). Thus, increasing the climate sensitivity means that the model goes through qualitatively and quantitatively the same amount of warming over a smaller range of CO₂ values. This implies that the potentially different climate sensitivity of past or future climates (e.g., Caballero & Huber, 2013) would not on its own cause the nature of sea ice bi-stabilities to change.

Figure 4g shows that the temperature of the mid-latitude ocean significantly affects the climate of the Arctic, but again barely affects the bi-stability of sea ice in the Arctic. Heat flux from the mid-latitude ocean is a major source of heat to the Arctic, so increasing the temperature of the mid-latitudes warms the overall Arctic climate significantly and shifts the regime where sea ice is supported to lower CO₂ values. As the mid-latitude ocean temperature increases, we also see a slight narrowing of the CO₂ range that leads to winter and summer sea-ice bi-stabilities (narrowing of the horizontal width of pink and purple color patches when moving up in panel g). We interpret this as a direct result of the fact that the ocean meridional heat flux was found to be a key factor in suppressing the tendency to bi-stability in Figure 3 which tends to warm the cold initial condition more than the warm initial condition. While increasing the midlatitude ocean temperature would increase the restoring heat flux on both initial conditions equally, it would make the meridional heating term larger in comparison to the other heating sources that govern the evolutions of the two initial conditions. In other words, higher midlatitude ocean temperatures simply mean that the meridional heat flux suppressing differences in the two ICs can more easily outweigh the positive feedbacks that tend to enhance differences in the two ICs, thus reducing the bi-stability. This suggests that climates with a low equator-to-pole temperature gradient favor Arctic sea-ice bi-stability. However, in Earth's past climate, such reduced equator-to-pole temperature gradient configurations have only occurred in overall very warm climates (such as the Eocene) where the climate would likely be very far from any bi-stable sea ice regime.

In the final results panel of Figure 4 (panel h), we see how the sea-ice stability changes as a function of the latitude at which we place our model grid box (the latitude controls the seasonal cycle of insolation, see Section 2). Interestingly, while the width of winter sea-ice bi-stability (pink and purple colors combined) is quite insensitive to the choice of latitude, the summer bi-stability width (purple color only) decreases as we move to higher latitudes. To understand this, we explain why the cold initial condition is less sensitive to latitude than the warm initial condition. The insensitivity of the CO₂ value of the transition in the cold initial condition from perennial ice to seasonal ice coverage is seen as the relatively vertical line separating the purple and pink colors near 400 ppm. This insensitivity can be explained by the cold initial condition starting out ice-covered (with a default ice-albedo of 0.725) and reflecting most of the insolation that reaches the surface, such that changes to the incoming insolation from changing latitude don't have a large impact. On the other hand, the warm initial condition starts out ice-free with a low albedo and thus absorbs most incoming insolation. Thus moving to lower latitudes significantly warms the warm initial condition, requiring lower CO₂ values to develop any initial ice. The bottom line is that factors that increase insolation and, therefore, the ice-albedo feedback, favor summer sea ice bi-stability, but such factors don't influence the winter sea ice bi-stability as much. Unintuitively, however, as we will discuss later, this does not mean that a winter bi-stability can exist without the ice-albedo feedback.

Examining all the panels together, a few salient features emerge. First, we re-emphasize that winter sea-ice bi-stability (perennial or seasonal ice coverage co-existing with perennial ice-free conditions at the same parameter values, shown by pink and purple colors) is a very robust feature across all model parameter ranges that we

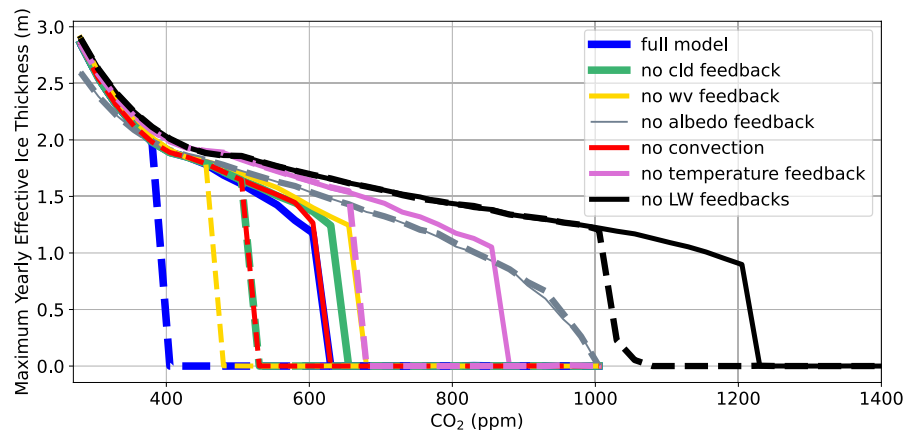


Figure 6. Maximum ice thickness (winter) versus CO_2 at steady-state for several different experiments. Dashed lines correspond to warm initial condition runs while solid lines correspond to cold initial condition runs. The hysteresis loop for a given experiment is seen by tracing the solid and then the dashed line—no such loop exists for the “no albedo feedback” experiment, pictured in grey, which has only one stable solution.

investigated. That is, this bi-stability occurs in some CO_2 range for almost all values of each of the parameters we considered (we also studied the sensitivity of winter bi-stability to other model parameters not shown here, but those did not demonstrate any notable influence on winter bi-stability). Surprisingly, summer sea-ice bi-stability (co-existence of perennial ice coverage and perennial ice-free conditions, shown by purple colors) also occurs for a significant portion of what might be considered realistic parameter combinations, similar to some previous modeling work (Eisenman, 2012; Eisenman & Wettlaufer, 2009). In this case, while such a bi-stability occurs in every panel of Figure 4 and for our default parameter choices (horizontal green line), it typically occurs for a narrower range of CO_2 and disappears under small changes from the default of some parameters (e.g., a small decrease in bare ice albedo, or a reduction of the LW emissivity of convective clouds). While (Eisenman, 2012) found that most cases of winter bi-stability also have an accompanying summer bi-stability, we find that winter bi-stability without summer sea ice bi-stability (i.e., bi-stability between seasonal ice and ice-free conditions) is the more prevalent case across all the parameter regimes (indicated by the pink color).

Finally, we also note the absence of any parameter combination that leads to summer sea ice bi-stability without winter bi-stability (i.e., bi-stability where the solution would converge to either perennial ice coverage or to a seasonal ice cover), which would have appeared as a mixed blue/white color in Figure 4. This follows from our work and previous studies (e.g., Bathiany et al., 2016; Eisenman, 2012) that find winter sea ice to always be more prone to bi-stability, and to respond more abruptly to CO_2 increases than summer sea ice. This suggests that any scenarios that lead to a summer sea ice bi-stability will likely also cause a winter sea-ice bi-stability. Abrupt sea ice changes can be related to bi-stability as we will discuss next, because they indicate the presence of positive feedback mechanisms that enhance small perturbations and large differences between two initial conditions.

3.3. Causes of Abrupt Sea Ice Loss

In this section, we examine what physical mechanisms set the abruptness of sea ice loss with respect to CO_2 . That is, we calculate the (seasonal) steady state for different values of CO_2 and examine the width of the range of CO_2 values over which the sea ice is abruptly lost, as well as the magnitude of sea ice loss that occurs during this abrupt period. The abruptness of sea ice loss has many implications, as a transition to ice-free conditions that is abrupt could reduce the ability to adapt to new Arctic conditions. While abrupt sea ice loss is often associated with a tipping point caused by a transition from a parameter regime of bi-stability to one of mono-stability, we note that an abrupt sea ice loss without bi-stability is possible (i.e., Bathiany et al., 2016), as are different magnitudes of tipping points from a bifurcation, depending on the size of the jump between the two stable solutions. Thus, the connection between the abruptness of sea ice loss and the bi-stability of sea ice deserves further investigation.

In Figure 6 we show the steady-state winter sea ice effective thickness across a range of CO_2 values for several different mechanism denial experiments (see Section 2 for how each mechanism denial experiment is

implemented). We show both the cold initial condition (solid lines) and the warm initial condition (dashed lines) steady-states, though in the discussion that follows, we focus more on the cold initial condition for its relevance to future global warming.

First, we note the remarkable similarity of the steepness of winter sea ice loss across most of the experiments. All experiments show a steepening of winter sea ice loss during the disappearance of the last 1 m of ice thickness over about 25–50 ppm of CO₂ increase. The most notable reduction in abruptness occurs for the experiment where we suppress the SAF, which is the only mechanism denial experiment that eliminated the winter sea-ice bifurcation. We would expect this experiment to have the most gradual sea ice loss since the loss is *not* governed by a bifurcation in this case, and while it is the most gradual loss seen in Figure 6, it still shows some acceleration during the last 1 m of loss.

Suppressing the water vapor feedback has a minimal effect (compare the yellow line to the blue line), slightly narrowing the CO₂ range of bi-stability and shifting the CO₂ threshold of the tipping point higher. Both of these results are to be expected as the water vapor feedback has a warming effect that should also be stronger in the warm IC.

Turning off atmospheric convection entirely and turning off the convective cloud feedback have nearly identical effects (compare the red and green lines in Figure 6), indicating that the main effect of convection on the modeled climate is through the convective cloud feedback. Without each of these feedbacks, the bi-stable regime narrows to only higher CO₂ values, but the magnitude of the sudden sea ice loss is not altered. This indicates that convective processes contribute to bi-stability but do not play a major role in driving the abruptness of Arctic sea ice loss in this model, contrary to suggestions by previous work (Abbot & Tziperman, 2008; Abbot et al., 2009).

We note a slightly more gradual sea ice loss (compared to the full model) in two longwave feedback denial experiments, the “no temperature feedback” experiment (pink lines) and the “no longwave feedback” experiment (black lines). In the experiment with temperature feedbacks turned off, atmospheric emissivity has all of its components (CO₂, water vapor, and convective cloud contributions), but the atmospheric temperature used to calculate longwave downwelling radiation that reaches the surface is fixed to its daily seasonal climatology calculated at 280 ppm of CO₂. In this experiment, the CO₂ range of bi-stability is shifted to much higher values (indicating significant cooling due to the suppression of the temperature feedback), and the tipping point is slightly smaller in magnitude than in the full model. This points to the interesting result that mechanisms that cool the climate overall can also lead to a smaller tipping point because they shift the bifurcation to a larger CO₂ that has a lower sea ice thickness value.

In the experiment where all longwave feedbacks are suppressed, the temperature used to calculate longwave warming of the surface is fixed as described above, and water vapor and convective clouds are also no longer included in the calculation of emissivity. In this configuration, changes to surface longwave downwelling radiation can only occur through increases to the CO₂-dependent LW emissivity. This shifts the sea ice tipping point to even higher CO₂ values and slightly narrows the CO₂ range of bi-stability. After the SAF, longwave feedbacks taken altogether have the most influence on the CO₂ threshold of the sea ice tipping point, and reveal yet another factor influencing bi-stability that we could not have identified from the experiments used in Figure 4. The importance of clear-sky longwave feedbacks in setting the abruptness of winter Arctic sea ice loss had been identified previously by Hankel and Tziperman (2021), but the relative contribution of water vapor versus temperature effects was unknown, as was the influence of these mechanisms on sea ice bi-stability. Here, we were able to exploit our simple modeling framework to show that while temperature changes can affect the sea-ice bi-stability much more than the water vapor feedback, a much greater change in the region of bi-stability occurs when their effects are taken together, as seen by the black lines in Figure 6. This can be understood by the fact that emissivity changes and atmospheric temperature changes have a multiplicative effect on surface longwave downwelling radiation.

Given the importance of longwave radiative feedbacks, we would like to know whether the temperature and moisture increases that drive increases in longwave downwelling have a remote or local source. To test this, we suppress all remote feedbacks simultaneously by setting the tropospheric and boundary layer moisture and temperature meridional fluxes to their values at 280 ppm. This means that all subsequent atmospheric warming and moistening of the Arctic atmosphere as CO₂ increases comes from local processes alone. We find that suppressing remote feedbacks does not change the bi-stability of the simulated climate at all (not shown), indicating that most of the temperature and moisture longwave feedbacks that occur in this model configuration are

due to exchanges between the local ocean, ice, and atmosphere. This is the result we expected given our findings in Section 2.6 that poleward atmospheric heat transport barely changed between preindustrial and two-times preindustrial conditions. However, if our model better represented the increase in poleward moisture transport under increased CO₂ that is predicted by other studies using GCMs (Graversen & Burtu, 2016; Graversen & Langen, 2019; Hwang et al., 2011; Kay et al., 2012; Yoshimori et al., 2014), we may expect this result to change. In particular, given that Graversen and Langen (2019) found enhanced latent heat transport to contribute modestly to Arctic sea ice loss and to enhanced water vapor and cloud feedbacks, we predict that the sea ice regimes would shift to higher CO₂ values and exhibit more narrow bi-stability when remote feedbacks are suppressed in such a case.

All of the experiments above eliminate the very small range of summer sea-ice bi-stability that occurs in the default parameter regime (see Figure S5 in Supporting Information S1). Most of the experiments have little effect on the abruptness or even the CO₂ value of summer sea ice loss, which occurs around 400 ppm in the full model. The exceptions are the temperature longwave feedback suppression and water vapor feedback suppression experiments which shift summer sea ice loss to slightly to about 425 ppm, and the total longwave feedback suppression experiment which shifts the summer sea ice loss to 475 ppm. This result points to a critical need to evaluate changes to lower atmospheric temperature and surface longwave downwelling radiation in the current Arctic climate in order to better understand and predict the exact timing of summer sea ice loss.

Overall, we find that multiple positive feedback mechanisms examined here influence the width and CO₂ range of sea ice bi-stability much more than they influence the abruptness of Arctic sea ice loss with greenhouse warming. When we did identify slightly more gradual Arctic sea ice loss, it was due to either the elimination of the winter sea ice bifurcation (as in the suppressed SAF experiment), or a shift in the sea ice bifurcation to higher CO₂ values where the cold steady-state had less sea ice, thus reducing the magnitude of the tipping point. The fact that the suppressed ice-albedo feedback experiment was the only one that eliminated the winter sea-ice bi-stability further highlights the crucial role this mechanism plays in allowing the two initial conditions to evolve to different steady states, and provides further evidence for its role in the different summer/winter sea ice equilibrium structures discussed earlier.

4. Discussion and Conclusions

In this work, we introduced a novel model of the Arctic climate that included both sea ice thermodynamics and atmospheric feedbacks in a simple framework. By running this model under a broad range of parameters, we exhaustively examined all local mechanisms that influence sea ice stability, found new bi-stability regimes and mechanisms, and interpreted the results of past studies on Arctic sea ice stability in light of these mechanisms.

Winter sea-ice bi-stability and an associated tipping point (in the sense of a bifurcation of the steady state) in winter sea ice with increased CO₂ were extremely robust features of this model, consistent with previous studies (Abbot & Tziperman, 2008; Abbot et al., 2009; Eisenman, 2012; Eisenman & Wettlaufer, 2009). In addition to the known shortwave SAF, we find that features that enhanced the bi-stability of winter Arctic sea ice (by widening the CO₂ range over which bi-stability occurs) included an increase in ocean mixed layer depth, an increase in the timescale of meridional ocean heat transport, and an increase in the longwave forcing of convective clouds. One of the very few parameter changes that could eliminate the winter sea-ice bi-stability was a large decrease in the timescale of meridional heat fluxes. This may potentially be related to the results of Wagner & Eisenman (2015)—who found that adding a continuous meridional dimension in a model without atmospheric feedbacks eliminated the winter sea ice bifurcation—since it also relates to the negative feedback mechanism of heat diffusion. Surprisingly, increasing the atmospheric albedo (to represent the formation of low summer clouds) has almost no effect on the winter sea-ice bi-stability, suggesting that the presence of low clouds may not disrupt the effectiveness of the SAF.

Many previous studies have also investigated the possibility of a summer sea ice bifurcation (Abbot, 2014; Eisenman, 2012; Eisenman & Wettlaufer, 2009; Holland et al., 2006; Tietsche et al., 2011; Wadhams, 2012), which is expected to occur much earlier than a winter bifurcation if it exists. There has been no clear consensus on this topic, with some simple models (Eisenman, 2012; Eisenman & Wettlaufer, 2009) and observational evidence (Wadhams, 2012) pointing toward the existence of summer sea ice bi-stability, while GCM studies (Armour et al., 2011; Ridley et al., 2012; Tietsche et al., 2011) typically find summer sea ice loss to be reversible.

We find that summer sea ice bi-stability can occur for some realistic parameter combinations (including our default parameters) but typically extends over a much smaller CO₂ range and exhibits more gradual sea ice loss. These results suggest that the irreversibility of summer sea ice loss could occur on small, local scales in areas of the Arctic with the appropriate conditions (which we've identified here as lower latitudes, minimal low cloud coverage, stronger convective processes, a deeper mixed layer, and less oceanic meridional heating) but may be less likely to occur on an Arctic-wide scale. Additionally, we find that even when summer sea ice is bi-stable, it doesn't undergo a large tipping-point-like drop at a threshold CO₂ value. Rather, the steady solution obtained from the cold initial condition smoothly evolves toward zero summer sea ice as CO₂ increases until it merges with the warm initial condition (see dashed blue line in Figure 5b). This is consistent with the prediction of CMIP5 models that summer sea ice should decline fairly smoothly under realistic future CO₂ increases (Hezel et al., 2014) but highlights the important point that such smooth decline does not preclude the existence of bi-stability and irreversibility.

Our results may help explain the abruptness of winter Arctic sea ice loss in GCMs. The insensitivity of sea ice loss abruptness in our mechanism denial experiments is somewhat surprising given the results of Hankel and Tziperman (2021) that found that positive feedback strength correlated with the abruptness of winter sea ice loss across six GCMs run in the CMIP5 RCP8.5 experiments. However, the mechanisms that did have a small influence on the abruptness of sea ice loss in the model used here (the SAF and clear-sky longwave feedbacks) are the same as those found by Hankel and Tziperman (2021) to play the biggest role in GCMs, suggesting the robust importance of those mechanisms. Finally, the fact that the one experiment (suppressed SAF) that did not exhibit a tipping point still showed an acceleration of sea ice loss indicates some roles for non-feedback mechanisms in causing abrupt sea ice loss, such as the freezing point mechanism proposed by Bathiany et al. (2016).

In GCMs run in the CMIP5 RCP8.5 Scenario, some models demonstrated an extremely large and abrupt loss of Arctic winter sea ice, while others exhibited a nearly linear, slower, and smoother decline (Hankel & Tziperman, 2021; Hezel et al., 2014). The fact that our model cannot reproduce this range of abruptness seen across GCMs suggests that other explanations for the inter-model variance besides the role of local positive feedbacks need to be considered. Our model has only a single grid box, possibly representing a relatively small domain within the Arctic. A more gradual sea ice loss could be caused by many smaller Arctic regions undergoing abrupt sea ice loss sequentially rather than simultaneously. This could eliminate an Arctic-wide winter sea ice jump via a mechanism that is different from the results of Wagner and Eisenman (2015), who included a meridional spatial dimension in their model.

Another possible mechanism for enhanced inter-model variability in the abruptness of sea ice loss across GCMs involves stochastic forcing. Stochastic forcing in a mono-stable system could cause sea ice to decline more gradually, as the sea ice would decline in a noisy, non-monotonic way, while it would be unlikely to change the abruptness of sea ice loss in a bi-stable system, instead making the system jump to the new steady-state prematurely and monotonically (by randomly pushing the system into the basin of attraction of the zero-sea ice solution). Thus, if some GCMs have bi-stable sea ice while others don't, stochastic noise could enhance the difference in sea ice loss abruptness between such models. In addition, GCMs usually have multiple sea ice thickness categories within each grid box, where different proportions of the ice fraction can be assigned different thicknesses (e.g., Horvat & Tziperman, 2015), while our model represents one ice thickness value for the whole domain. Multiple thickness categories could allow for more gradual sea ice loss on the grid-box level, as the thinnest category of sea ice would undergo its abrupt loss before the thicker categories. This could enhance the differences in the abruptness of sea ice loss found here across different mechanism denial experiments. In sum, the difference between our model's range of sea ice loss abruptness and that of GCMs helps narrow down the possible set of mechanisms that could cause such inter-model variance in GCMs.

We also comment on how our results address the connection between climate model complexity and sea ice stability. Wagner and Eisenman (2015) found that the addition of a continuous meridional dimension to a thermodynamic sea ice model similar to the one used here (but without dynamic atmospheric feedbacks) can destroy sea ice bi-stability, suggesting that bi-stability was an artifact of an overly simplified model. However, here we find a complicated picture where several different mechanisms that enhance or suppress differences in the two initial conditions (including atmospheric ones not explicitly represented in Wagner and Eisenman (2015)) compete with each other to establish either one or multiple sea ice steady-states, and the outcome depends highly on the specific combination of parameter choices used. In particular, simplifying our model by turning off various

features (such as atmospheric convection or longwave feedbacks) actually eliminated the small range of summer sea ice bi-stability. This suggests that sea ice stability does not necessarily depend only on model complexity, but rather on the exact balance of the positive and negative feedback mechanisms a model represents.

Finally, we highlight how the manipulability of our simple model framework allowed us to identify key atmospheric mechanisms for the timing and abruptness of sea ice loss that would be hard to isolate in an atmospheric column such as that used by Abbot and Tziperman (2008), and certainly in a full complexity GCM. Specifically, we found that convective processes can narrow the CO₂ range of sea ice bi-stability, but barely affect the CO₂ threshold of the sea ice tipping point as CO₂ increases. Meanwhile, longwave temperature feedbacks play a major role in the timing of sea-ice loss and a minor role in the stability and abruptness of winter sea-ice loss. These results may help inform future observational and GCM-modeling studies of the Arctic that aim to improve sea ice projections; in particular, they indicate the importance of observing the lower atmospheric temperature, onsets of convection, and increases to surface longwave downwelling radiation in order to assess the evolving potential for abrupt sea ice loss. Our results also show that summer sea ice bi-stability is favored in the lower latitudes, where present-day sea ice loss is already occurring. This suggests that observational and modeling studies could look for signs of irreversibility in current summer sea ice loss, which would likely imply the irreversibility of winter sea ice loss as well.

Data Availability Statement

An implementation in Python 3.7 of the Arctic sea-ice box model with atmospheric feedbacks described in this work can be found at <https://doi.org/10.5281/zenodo.7983226> (Hankel, 2023). The data from CanESM5 used for model validation is distributed by the Earth System Grid Federation (Cinquini et al., 2014) and can be downloaded at <https://esgf-node.llnl.gov/search/cmip6/>.

Acknowledgments

This work was funded by DOE Grant DE-SC0023134. ET thanks the Weizmann Institute for its hospitality during parts of this work.

References

- Abbot, D. S. (2014). Resolved snowball Earth clouds. *Journal of Climate*, 27(12), 4391–4402. <https://doi.org/10.1175/jcli-d-13-00738.1>
- Abbot, D. S., Silber, M., & Pierrehumbert, R. T. (2011). Bifurcations leading to summer Arctic sea ice loss. *Journal of Geophysical Research*, 116(D19), D19120. <https://doi.org/10.1029/2011jd015653>
- Abbot, D. S., & Tziperman, E. (2008). Sea ice, high-latitude convection, and equable climates. *Geophysical Research Letters*, 35(3), L03702. <https://doi.org/10.1029/2007gl032286>
- Abbot, D. S., Walker, C., & Tziperman, E. (2009). Can a convective cloud feedback help to eliminate winter sea ice at high CO₂ concentrations? *Journal of Climate*, 22(21), 5719–5731. <https://doi.org/10.1175/2009JCLI2854.1>
- Armour, K., Eisenman, I., Blanchard-Wrigglesworth, E., McCusker, K., & Bitz, C. (2011). The reversibility of sea ice loss in a state-of-the-art climate model. *Geophysical Research Letters*, 38(16), L16705. <https://doi.org/10.1029/2011gl048739>
- Bathiany, S., Notz, D., Mauritsen, T., Raedel, G., & Brovkin, V. (2016). On the potential for abrupt Arctic winter sea ice loss. *Journal of Climate*, 29(7), 2703–2719. <https://doi.org/10.1175/jcli-d-15-0466.1>
- Bitz, C. M., Holland, M., Hunke, E., & Moritz, R. (2005). Maintenance of the sea-ice edge. *Journal of Climate*, 18(15), 2903–2921. <https://doi.org/10.1175/jcli3428.1>
- Boeke, R. C., & Taylor, P. C. (2018). Seasonal energy exchange in sea ice retreat regions contributes to differences in projected Arctic warming. *Nature Communications*, 9(1), 1–14. <https://doi.org/10.1038/s41467-018-07061-9>
- Caballero, R., & Huber, M. (2013). State-dependent climate sensitivity in past warm climates and its implications for future climate projections. *Proceedings of the National Academy of Sciences of the United States of America*, 110(35), 14162–14167. <https://doi.org/10.1073/pnas.1303365110>
- Cinquini, L., Crichton, D., Mattmann, C., Harney, J., Shipman, G., Wang, F., et al. (2014). The Earth system grid federation: An open infrastructure for access to distributed geospatial data [Dataset]. *Future Generation Computer Systems*, 36, 400–417. <https://doi.org/10.1016/j.future.2013.07.002>
- Comiso, J. C., & Parkinson, C. L. (2004). Satellite observed changes in the Arctic. *Physics Today*, 57(8), 38–44. <https://doi.org/10.1063/1.1801866>
- Eisenman, I. (2007). Arctic catastrophes in an idealized sea ice model. *Program of Studies: Ice*, 133–161. (Geophysical Fluid Dynamics Program).
- Eisenman, I. (2012). Factors controlling the bifurcation structure of sea ice retreat. *Journal of Geophysical Research*, 117(D1), D01111. <https://doi.org/10.1029/2011jd016164>
- Eisenman, I., & Wettlaufer, J. S. (2009). Nonlinear threshold behavior during the loss of Arctic sea ice. *Proceedings of the National Academy of Sciences of the United States of America*, 106(1), 28–32. <https://doi.org/10.1073/pnas.0806887106>
- Emanuel, K. A. (1994). *Atmospheric convection*. Oxford University Press.
- Ferreira, D., Marshall, J., & Rose, B. (2011). Climate determinism revisited: Multiple equilibria in a complex climate model. *Journal of Climate*, 24(4), 992–1012. <https://doi.org/10.1175/2010jcli3580.1>
- Ghil, M., & Childress, S. (1987). *Topics in geophysical fluid dynamics: Atmospheric dynamics, dynamo theory and climate dynamics*. Springer-Verlag.
- Graversen, R. G., & Burtu, M. (2016). Arctic amplification enhanced by latent energy transport of atmospheric planetary waves. *Quarterly Journal of the Royal Meteorological Society*, 142(698), 2046–2054. <https://doi.org/10.1002/qj.2802>
- Graversen, R. G., & Langen, P. L. (2019). On the role of the atmospheric energy transport in 2x CO₂-induced polar amplification in CESM1. *Journal of Climate*, 32(13), 3941–3956. <https://doi.org/10.1175/jcli-d-18-0546.1>

- Hahn, L. C., Armour, K. C., Zelinka, M. D., Bitz, C. M., & Donohoe, A. (2021). Contributions to polar amplification in CMIP5 and CMIP6 models. *Frontiers in Earth Science*, 9, 710036. <https://doi.org/10.3389/feart.2021.710036>
- Hankel, C. (2023). Arctic sea ice box model with 2-layer atmosphere [Software]. Zenodo. <https://doi.org/10.5281/zenodo.7983226>
- Hankel, C., & Tziperman, E. (2021). The role of atmospheric feedbacks in abrupt winter Arctic sea ice loss in future warming scenarios. *Journal of Climate*, 34(11), 4435–4447. <https://doi.org/10.1175/jcli-d-20-0558.1>
- Hartmann, D. L. (2015). *Global physical climatology*. In (Vol. 103, chap. Chapter 2). Newnes.
- Hezel, P., Fichefet, T., & Massonnet, F. (2014). Modeled Arctic sea ice evolution through 2300 in CMIP5 extended RCPs. *The Cryosphere*, 8(4), 1195–1204. <https://doi.org/10.5194/tc-8-1195-2014>
- Hibler, W. D., III. (1979). A dynamic thermodynamic sea ice model. *Journal of Physical Oceanography*, 9(4), 815–846. [https://doi.org/10.1175/1520-0485\(1979\)009<0815:adtsim>2.0.co;2](https://doi.org/10.1175/1520-0485(1979)009<0815:adtsim>2.0.co;2)
- Holland, M. M., Bitz, C. M., & Tremblay, B. (2006). Future abrupt reductions in the summer Arctic sea ice. *Geophysical Research Letters*, 33(23), L23503. <https://doi.org/10.1029/2006gl028024>
- Holland, M. M., Bitz, C. M., Tremblay, L.-B., & Bailey, D. A. (2008). The role of natural versus forced change in future rapid summer Arctic ice loss. *Arctic Sea Ice Decline: Observations, Projections, Mechanisms, and Implications*, 180, 133–150. <https://doi.org/10.1029/180gm10>
- Horvat, C., & Tziperman, E. (2015). A prognostic model of the sea ice floe size and thickness distribution. *The Cryosphere*, 9(6), 2119–2134. <https://doi.org/10.5194/tc-9-2119-2015>
- Hwang, Y.-T., Frierson, D. M., & Kay, J. E. (2011). Coupling between Arctic feedbacks and changes in poleward energy transport. *Geophysical Research Letters*, 38(17), L17704. <https://doi.org/10.1029/2011gl048546>
- Kay, J. E., & Gettelman, A. (2009). Cloud influence on and response to seasonal Arctic sea ice loss. *Journal of Geophysical Research*, 114(D18), D18204. <https://doi.org/10.1029/2009jd011773>
- Kay, J. E., Holland, M. M., Bitz, C. M., Blanchard-Wrigglesworth, E., Gettelman, A., Conley, A., & Bailey, D. (2012). The influence of local feedbacks and northward heat transport on the equilibrium Arctic climate response to increased greenhouse gas forcing. *Journal of Climate*, 25(16), 5433–5450. <https://doi.org/10.1175/jcli-d-11-00622.1>
- Kay, J. E., L'Ecuyer, T., Chepfer, H., Loeb, N., Morrison, A., & Cesana, G. (2016). Recent advances in Arctic cloud and climate research. *Current Climate Change Reports*, 2(4), 159–169. <https://doi.org/10.1007/s40641-016-0051-9>
- Keen, A., Blockley, E., Bailey, D. A., Bolding Debernard, J., Bushuk, M., Delhaye, S., et al. (2021). An inter-comparison of the mass budget of the Arctic sea ice in CMIP6 models. *The Cryosphere*, 15(2), 951–982. <https://doi.org/10.5194/tc-15-951-2021>
- Lenton, T. M. (2012). Arctic climate tipping points. *Ambio*, 41(1), 10–22. <https://doi.org/10.1007/s13280-011-0221-x>
- Li, C., Notz, D., Tietsche, S., & Marotzke, J. (2013). The transient versus the equilibrium response of sea ice to global warming. *Journal of Climate*, 26(15), 5624–5636. <https://doi.org/10.1175/jcli-d-12-00492.1>
- Morrison, A., Kay, J. E., Frey, W., Chepfer, H., & Guzman, R. (2019). Cloud response to Arctic sea ice loss and implications for future feedback in the CESM1 climate model. *Journal of Geophysical Research: Atmospheres*, 124(2), 1003–1020. <https://doi.org/10.1029/2018jd029142>
- Neale, R. B., Chen, C.-C., Gettelman, A., Lauritzen, P. H., Park, S., Williamson, D. L., et al. (2010). Description of the NCAR community atmosphere model (CAM 5.0). NCAR Technical Note NCAR/TN-486+ STR, 1(1), 1–12.
- Nghiem, S., Rigor, I., Perovich, D., Clemente-Colón, P., Weatherly, J., & Neumann, G. (2007). Rapid reduction of Arctic perennial sea ice. *Geophysical Research Letters*, 34(19), L19504. <https://doi.org/10.1029/2007gl031138>
- Notz, D. (2009). The future of ice sheets and sea ice: Between reversible retreat and unstoppable loss. *Proceedings of the National Academy of Sciences of the United States of America*, 106(49), 20590–20595. <https://doi.org/10.1073/pnas.0902356106>
- Notz, D., & Stroeve, J. (2016). Observed Arctic sea-ice loss directly follows anthropogenic CO₂ emission. *Science*, 354(6313), 747–750. <https://doi.org/10.1126/science.aag2345>
- Ridley, J., Lowe, J., & Hewitt, H. (2012). How reversible is sea ice loss? *The Cryosphere*, 6(1), 193–198. <https://doi.org/10.5194/tc-6-193-2012>
- Sayag, R., Tziperman, E., & Ghil, M. (2004). Rapid switch-like sea ice growth and land ice-sea ice hysteresis. *Paleoceanography*, 19, PA1021. <https://doi.org/10.1029/2003PA000946>
- Skific, N., & Francis, J. A. (2013). Drivers of projected change in Arctic moist static energy transport. *Journal of Geophysical Research: Atmospheres*, 118(7), 2748–2761. <https://doi.org/10.1002/jgrd.50292>
- Stroeve, J., & Notz, D. (2018). Changing state of Arctic sea ice across all seasons. *Environmental Research Letters*, 13(10), 103001. <https://doi.org/10.1088/1748-9326/aade56>
- Stroeve, J., Serreze, M., Drobot, S., Gearheard, S., Holland, M., Maslanik, J., et al. (2008). Arctic sea ice extent plummets in 2007. *Eos, Transactions American Geophysical Union*, 89(2), 13–14. <https://doi.org/10.1029/2008eo020001>
- Strogatz, S. (1994). *Nonlinear dynamics and chaos*. Westview Press.
- Tietsche, S., Notz, D., Jungclaus, J., & Marotzke, J. (2011). Recovery mechanisms of Arctic summer sea ice. *Geophysical Research Letters*, 38(2), L02707. <https://doi.org/10.1029/2010gl045698>
- Tziperman, E. (2022). *Global warming science: A quantitative introduction to climate change and its consequences*. Princeton University Press.
- Tziperman, E., Toggweiler, J. R., Feliks, Y., & Bryan, K. (1994). Instability of the thermohaline circulation with respect to mixed boundary-conditions: Is it really a problem for realistic models. *Journal of Physical Oceanography*, 24(2), 217–232. [https://doi.org/10.1175/1520-0485\(1994\)024<0217:iottcw>2.0.co;2](https://doi.org/10.1175/1520-0485(1994)024<0217:iottcw>2.0.co;2)
- Wadhams, P. (2012). Arctic ice cover, ice thickness and tipping points. *Ambio*, 41(1), 23–33. <https://doi.org/10.1007/s13280-011-0222-9>
- Wagner, T. J., & Eisenman, I. (2015). How climate model complexity influences sea ice stability. *Journal of Climate*, 28(10), 3998–4014. <https://doi.org/10.1175/jcli-d-14-00654.1>
- Yang, H., Li, Q., Wang, K., Sun, Y., & Sun, D. (2015). Decomposing the meridional heat transport in the climate system. *Climate Dynamics*, 44(9–10), 2751–2768. <https://doi.org/10.1007/s00382-014-2380-5>
- Yoshimori, M., Abe-Ouchi, A., & Lañé, A. (2017). The role of atmospheric heat transport and regional feedbacks in the Arctic warming at equilibrium. *Climate Dynamics*, 49(9–10), 3457–3472. <https://doi.org/10.1007/s00382-017-3523-2>
- Yoshimori, M., Watanabe, M., Abe-Ouchi, A., Shiogama, H., & Ogura, T. (2014). Relative contribution of feedback processes to Arctic amplification of temperature change in MIROC GCM. *Climate Dynamics*, 42(5–6), 1613–1630. <https://doi.org/10.1007/s00382-013-1875-9>

References From the Supporting Information

- Eyring, V., Bony, S., Meehl, G. A., Senior, C. A., Stevens, B., Stouffer, R. J., & Taylor, K. E. (2016). Overview of the coupled model inter-comparison project phase 6 (CMIP6) experimental design and organization. *Geoscientific Model Development*, 9(5), 1937–1958. <https://doi.org/10.5194/gmd-9-1937-2016>